JOURNAL OF MATERIALS SCIENCE 32 (1997) 4463–4484

Review
Films of interstitial phases: synthesis and properties

R. A. ANDRIEVSKI
Institute for New Chemical Problems, Russian Academy of Sciences, Chernogolovka, Moscow Region, 142432, Russia

The effective preparation methods of transition metal carbide, nitride, boride, and hydride films (so-called interstitial phases (IPs)) are described. The different versions of PVD and CVD techniques are compared and discussed. Special attention is paid to the structure analysis of IP films. Physical and mechanical properties as well as recrystallization of these subjects, including multilayer ones, are analysed in detail. The development of new materials based on IP films is shown to parallel closely the progress in nanocrystalline materials science.

1. Introduction

As far as is known, the term "interstitial phases" (or interstitial alloys, interstitial compounds or Hagg compounds) dates back about 60 years after Hagg's [1] structural investigations of the systems of transition metal – light non-metallic elements (hydrogen, nitrogen, boron, carbon, etc.) when the location of these small atoms was first supposed and then proved in interstitial sites of simple metal sublattices. Typical examples of IP structures, such as sodium chloride type, in which the octahedral interstitial sites in a face-centred cubic metal array are occupied by carbon or nitrogen atoms, and calcium difluoride type, in which the tetrahedral ones in a similar array, are occupied by hydrogen atoms, are very well known. Boride structures are more complex and, in addition, the initial opinion on IPs as with compounds with a simple structure, has undergone a significant change and still stand only for some stoichiometric phases. The point is that the majority of nonstoichiometric IPs undergo ordering in the non-metallic sublattice and change their structural type from a simple to a more complex one. So the known Hagg rule on the ratio of the non-metallic atomic radius to that of the transition metal as a possibility for IP formation prediction has very limited application. Therefore, as has been shown [2], the term IP is more historical. Carbides, nitrides, hydrides, some monoxides (for example TiO), and partly borides of the III–VI period transition metals with metallic properties (such as electrical resistance temperature positive effect) are attributed to IPs by definition.

There are many monographs on IP preparation and properties (e.g. [2–21]), to say nothing of a large body of different collections. However, research on films has been on a very limited scale (e.g. [7]). This is mainly due to the fact that the extended studies of IP films which are currently an active area, has only been possible for the past 10–15 years following the development of advanced technology methods, such as arc evaporation and magnetron sputtering as well as plasma-assisted (or enhanced) CVD (PACVD or PECVD) technique. The wide application of IP films in tool and electronic materials has given impetus to the development of these researches. TiN films are a particular leader but in applications and publications. In the literature, hundreds of works are dedicated to titanium nitride films. Comprehensive reviews on this subject can be found (e.g. [22–27]). Some noteworthy books are dedicated to films and coatings (e.g. [28–31]). However, the topic of IP films as a whole seems not to be covered because the data on many other subjects (such as carbides, borides, hydrides, and nitrides other than TiN) are scattered throughout the literature, covering a range of application topics rather than particularly IP. It should be also noted that consideration of IP films deals not only with the surface engineering aspect, but it is strongly interlinked with the development of nanocrystalline materials [32, 33]. The above-mentioned circumstances are the reason for writing the present review.

2. Preparation

2.1. General considerations

We shall consider films with thicknesses up to several micrometres. As a rule, coatings with thicknesses up to several tens of micrometres and more will not be considered. It is common knowledge that the maximum thickness of a "thin" film is not well defined. However a value of 3–5 μm seems to be the most widely accepted. Such films may be prepared by numerous means which can be broadly classified into physical and chemical methods, with some variants (Table I). The present author points out that this classification is very conventional and in many ways it is similar to that for ultrafine powder preparation

TABLE I Main methods of IP film preparation

Group	Method	Variation	Compound
Physical	Thermal evaporation		
		Electron beam	Borides and carbides
		Laser	Nitrides and carbides
	Ion plating		
		Arc deposition	Nitrides and carbides
		Magnetron sputtering	Nitrides, borides, carbides and hydrides
		Ion-beam-assisted deposition and implantation	Nitrides and borides
Chemical	Deposition from gas phase		
		PACVD, PECVD, electron cyclotron resonance	Nitrides, carbides and borides
	Thermal decomposition		
		Gaseous and condense precursors	Nitrides and borides
	Nitriding and hydriding		
		Low-temperature versions and implantation	Nitrides and hydrides

[32, 33]. In many cases the preparation method is based on more than one basic principle and the boundary between them is often diffuse and poorly defined.

Chemical reactions have a profound impact in thermal evaporation and ion plating while the physical actions, such as plasma or laser are in considerable use for the acceleration of chemical reactions. In the pure state, the existing terms chemical vapour deposition (CVD) and physical vapour deposition (PVD) are mainly of historical significance. Table I does not claim to be an exhaustive classification. Some other PVD and CVD classifications also exist (e.g. [23, 24, 34]). So Table I includes only some of the main preparation methods. Conventional ones, such as simple evaporation in an inert/reactive atmosphere, simple sputtering, etc., are implied. One can see that nitride IPs can be produced by essentially all routes. Only low temperature routes, such as hydriding and magnetron sputtering can be used for hydride IPs because of their high dissociation pressure values. Carbide and boride IPs steer a middle course between nitride and hydride IPs. Let us consider some of the most popular methods at greater length.

2.2. Physical methods

2.2.1. Thermal evaporation

Because of the high melting temperature values for the majority of carbides, borides, and nitrides, the evaporation process by direct resistance and radiation is very seldomly used. The application of electron-beam evaporation (EBE) has been described as applied to carbide, boride and TiC/TiB_2 films [35]. This method was carried out at high substrate temperature (650–1600 °C); the deposition rate of the compound phase was up to 6 $\mu m\,min^{-1}$ and the total thickness of the condensates was up to 0.25–0.3 mm. The obtained properties were found not to be high; the maximum value of hardness was about 20–30 GPa. Thermal evaporation of metals or alloys in a reactive atmosphere (carburizing, nitriding, or hydriding) and especially activated reactive evaporation (ARE) is more popular for film preparation. The use of a glow discharge, thermoionic electron beam or arc heating in the ARE process for carbide and nitride film synthesis is known [24, 34, 36]. Laser reactive sputtering (LRS) of a niobium target in a carburizing atmosphere has been used to obtain NbC films [37]. The possibility of composition change must be taken into consideration in most cases of IP thermal evaporation in connection with their wide range of homogeneity and incongruent evaporation.

The vacuum thermal vapour deposition technique and electron beam evaporation are also used for intermetallic film preparation (e.g. FeTi, $LaNi_5$ and so on) followed by hydriding for hydride formation (e.g. [38, 39]).

2.2.2. Ion plating

The term ion plating, first used in the work [40], is applied to a family of deposition processes in which the substrate surface is subjected to a flux of ions before and during film growth (e.g. [41]). Arc deposition is of great use in the tool industry for the preparation of TiN and Ti(N,C) films. This method is called the cathodic arc plasma deposition (CAPD) in which a cathode arc is used as an evaporation source [41, 42]. The CAPD process is characterized as follows: (i) a very high percentage of the evaporated material is ionized, 30–100% depending on the source material; (ii) the ions in the emitted plasma are multiply charged; (iii) the emitted ions possess very high kinetic energies, 10–200 eV; (iv) the condensation rate is up to 1–3 $\mu m\,min^{-1}$ (usually several tenths of micrometres per minute). In most cases the CAPD process is performed in a reactive atmosphere using $Ar + N_2$ or $Ar + C_nH_m$ working gases, at a pressure of around 10^{-2} torr (1 Pa), and a metallic cathode (Ti, Zr, V, Mo, etc.). The main disadvantage of CAPD is the possible presence of heavier uncharged microparticles (microdroplets) in the plasma and respectively in the films. Some filtered CAPD processes have been proposed to eliminate this phenomenon based, for example, on using a magnetic flux tube to guide the plasma from the cathode around a curved plasma duct into the deposition chamber (e.g. [24, 43, 44]). There are also hybrid PVD technologies involving both multi-arc devices and simultaneous or

successive application of CAPD and magnetron sputtering to deposit multilayer/multicomponent films [45].

The latter is the more flexible method which permits the use not only of metallic cathodes but also carbide, boride, nitride, and mixed ones, and deposition at low temperatures (100–200 °C and lower). So the possibility of obtaining IP films with different compositions and structures (amorphous, nanocrystalline, etc.) is considerably greater as compared with thermal evaporation, CAPD and other methods. Another important advantage of the sputtering process is that the composition of a sputtered film as-deposited is the same as that of the target composition without further reaction [24]. There are many versions of magnetron sputtering such as the application of d.c. or r.f. sputtering, using inert and reactive working gases, bias voltage, and unbalanced magnetrons (e.g. [24, 26, 41]) although a percentage of the ionization and kinetic energy of the ions is lower in all versions than in the case of CAPD (respectively $< 10\%$ and up 10 eV) and the deposition rate is also not as high (usually lower than 0.1–0.2 $\mu m\,min^{-1}$). Magnetron sputtering deposition is controlled by various parameters, such as the surface temperature of the substrate, the total pressure and composition of the working gas, the substrate bias and ion current density, the deposition rate, etc. The ionization problem in different plasma assisted PVD systems has been analysed by Matthews *et al.* [46].

In recent times, the different systems of ion-beam-assisted deposition (IBAD) or ion-beam-enhanced deposition (IBED) have gained acceptance (e.g. [47, 48]). In these processes the film deposition is accompanied or enhanced by bombardment of the substrate by an energetic ion beam, i.e. the conventional deposition technique is combined with ion implantation which can drastically change the structure and properties of films, and produce films with some unique characteristics. For example, crystalline TiB_2 coatings with thicknesses up to 1 μm have been prepared by sputtering at room temperature with simultaneous high-energy heavy ion bombardment (320 keV Ar^{2+} or 320 keV Xe^{2+}) during the deposition [49]. Only amorphous TiB_2 deposits can be prepared under these conditions without dynamic ion mixing. On the other hand, N_2 bombardment during nitride film deposition leads to the formation of superstoichiometric compounds and changes the preferred orientation [47].

Some theoretical methods for the description of magnetron sputtering and IBAD have been proposed [50, 51]. In the latter, molecular dynamics simulation allowed the prediction of film surface smoothing and improvement of TiN stoichiometry.

2.3. Chemical methods

2.3.1. Deposition from gas phase

The conventional CVD technique with high-temperature gas reactions of type

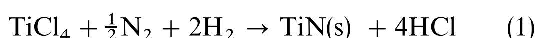

$$TiCl_4 + \tfrac{1}{2}N_2 + 2H_2 \rightarrow TiN(s) + 4HCl \qquad (1)$$

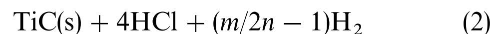

$$TiCl_4 + \tfrac{1}{n}C_nH_m + H_2 \rightarrow TiC(s) + 4HCl + (m/2n - 1)H_2 \qquad (2)$$

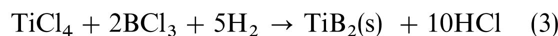

$$TiCl_4 + 2BCl_3 + 5H_2 \rightarrow TiB_2(s) + 10HCl \qquad (3)$$

persists to the present because of its economical benefit for many ordinary applications without any complicated demands for films and coatings. Reactions 1–3 are given as an overall view; there are many intermediate stages and all are complicated by impurity effects, and especially due to oxygen. A comprehensive review of CVD TiN coatings for wear-resistant applications has been published by Rebenne and Bhat [27]. Not only single layers of IPs but also different compositions and combinations of films, such as $Ti(C_xN_y)$, TiC/TiN, TiC/Al_2O_3, TiC/TiB_2, $TiC/Al_2O_3/TiN$ multilayers, etc., have been developed and commercialized to a significant degree [24, 27, 52].

In most cases the temperature interval for CVD films is between 900–1100 °C. Deposition rates of 0.03–0.2 $\mu m\,min^{-1}$ are typically used under these conditions. The quest to activate the CVD process and decrease the temperatures used has resulted in the use of plasma assistance (PACVD and PECVD) as well as laser-assisted CVD (LACVD) and electron cyclotron resonance (ECR). These versions are characterized by the following features [27, 53–60]:

(i) The deposition temperature decreases to 600–300 °C and below.
(ii) The deposition rates are equal to 10^{-3}–0.2 μm min^{-1}.
(iii) Not only $TiCl_4$, $N_2(NH_3)$ and C_6H_6(C_7H_{16} and similar hydrocarbons) but metalorganic compounds, such as tetrakis-dimethyl-amido titanium (TDMAT or TMT, $Ti(N(CH_3)_2)_4$), tetrakis-diethyl-amido titanium (TDEAT or TET, $Ti(N(C_2H_5)_2)_4$), and tetra-isopropoxide titanium (TIPT, $Ti(OCH(CH_3)_2)_4$) are commonly used as precursors because these latter have relatively high vapour pressures. These metalorganic precursors lead partly to carbonitride film formation.
(iv) As compared with conventional CVD the foregoing methods demand specific equipment and in most cases they are used in electronic applications.

For example, the scheme for TiN deposition, using chemical beams of TDMAT precursor and ECR plasma-activated nitrogen, includes the following [57]. The chamber base pressure is kept below 10^{-10} torr (1.3×10^{-8} Pa) and pressure during deposition is about 10^{-4} torr (1.3×10^{-2} Pa) and nitrogen, activated at the ECR cell, is the main gas. The flux value of TDMAT is 4×10^{14} molecules $cm^{-2}\,s^{-1}$. Films were deposited on Si wafers with oxidized surfaces, which were heated to 100 °C. It was shown that deposition rate, electrical resistivity and composition of films are changed when a d.c. bias is applied to the substrate. Positive ions are considered to be important in deposition and in improving film properties. The higher deposition rate (of about 5×10^{-4} $\mu m\,min^{-1}$)

and the lowest resistivity value were observed for a bias voltage of − 50 V for film compositions measured by X-ray photoelectron spectroscopy (XPS) *ex situ*. From these data the following film composition was calculated: ~ 42 at %Ti, ~ 42 at %N, ~ 10 at % C and ~ 6 at %O. Assuming the location of all non-metallic elements in the nitrogen sublattice the approximate formula $Ti(N_{0.72}C_{0.17}O_{0.11})_{1.38}$ may also be proposed for this composition. Satisfactory coatings were produced at the bases of blind holes in the substrate. There are two other ECR results which have demonstrated promising characteristics of this method. For example, the film resistivity was shown to decrease and low contamination of carbon and oxygen were also observed, however at the same time the deposition rates seems to be low and equalled only $(1-3)\times 10^{-3}\,\mu m\,min^{-1}$ (substrate temperature of 100–500 °C) [58–60].

As applied to groups 4 and 5 transition metal nitrides, the possibility of film synthesis has also been described using precursors such as homoleptic tetrakis dialkylamido metal complexes ($M(N(CH_3)_2)_n$) and ammonia at atmospheric pressure [61, 62]. In this case comparatively high growth rates (0.02–$0.2\,\mu m\,min^{-1}$), low substrate temperatures (200–400 °C) and low carbon and oxygen contaminations have been obtained. Atomic layer epitaxial growth of TiN thin films at 500 °C has also been described by alternately introducing $TiCl_4$ and NH_3 on the substrate employing a reducing zinc pulse after the $TiCl_4$ dose [63].

As is evident from the foregoing, CVD development is progressing rapidly, the accretion of data is continuing and by now to prefer any favourable method, which permits effective film deposition at low temperature, involves difficulties.

2.3.2. Thermal decomposition

No comprehensive information relating to thermal decomposition of gaseous precursors being transformed to IPs has been published. Thermal decomposition as applied to TiN formation from metalorganic precursors has been briefly discussed elsewhere [55]. The low-temperature deposition of titanium, zirconium and hafnium boride films by the thermal decomposition of the metal borohydrides is described by several investigators (e.g. [64–66]. Table II shows the decomposition analysis data for zirconium borohydride $Zr(BH_4)_4$ [66]. From these results it is obvious that it is possible to deposit boride at low temperatures in both amorphous and crystalline form. The latter is characteristic for films deposited on glass or silicon near the heating zone. Ultrafine powder (UFP) depositions which collected in the larger part of the tube were characterized by having a larger boron content and amorphous structure. The boron content increases with increasing temperature. The boron excess is likely to be connected with diborane decomposition

$$Zr(BH_4)_4 \rightarrow ZrB_2 + B_2H_6 + 5H_2 \qquad (4)$$

because the ratio $[H_2]/[B_2H_6]$ in the gas phase, as is evident from Table II, is larger than the theoretical value for Reaction 4. The presence of superstoichiometric boron content in borides prepared by a decomposition of borohydrides has also been shown in other works (e.g. [64, 65]).

Very little published information is available on the use of liquid precursors. Films of $TiC_{0.8}N_{0.2}$ with a thickness of 0.6 μm have been obtained by dipping into a solution of $Ti(NR_2)_4$ polymer followed by annealing in inert atmosphere at 500–1000 °C [67].

2.3.3. Nitriding and hydriding

These methods are performed in different versions: nitrogen ion implantation of evaporated thin metallic films or surface layers [68, 69], nitriding surface layers in microwave discharge [70], low temperature (400 °C) nitriding by hydrazine [71], hydriding films in soft conditions including electrochemical and magnetron sputtering cases [38, 39, 72, 73]. However, with the exception of hydrides all known examples do not seem to be so promising as compared with other methods of nitride films preparation. For hydride films this method together with magnetron sputtering in reactive atmosphere may be the only ones possible but they have not been investigated in detail.

3. Composition, structure, defects, and bonding

3.1. General characteristics

It is common knowledge that small film thickness causes pertinent methods of their characterization. This is especially true in regard to composition and defect analyses. Many methods, such as XPS, Auger electron spectroscopy (AES), X-ray diffraction (XRD) analysis, scanning and transmission electron microscopy (SEM and TEM) including high resolution (HR) versions, energy disperse spectroscopy (EDS),

TABLE II Analytical data for decomposition product of $Zr(BH_4)_4$ vapours at 250–350 °C ($t = 5$ h)

Temperature (°C)	Deposition type	B/Zr	Lattice parameters (nm)		$[H_2]/[B_2H_6]$ in gas phase
			a	*c*	
250	–	–	–	–	–
300	UFP	2.76	Amorphous		9
300	Film	2.03	0.3167	0.3528	9
350	UFP	3.74	Amorphous		12
350	Film	2.15	0.3165	0.3534	12

TABLE III Composition of some IP films prepared by different methods (DCMRS, d.c. magnetron reactive sputtering; ThD, thermal decomposition; RFMNRS and RFMRS, r.f. magnetron non-reactive sputtering and r.f. magnetron reactive sputtering)

Preparation method	Composition	Characterization method
LRS [37]	$NbC_{0.75–0.98}$	XPS
ECR plasma [57]	$Ti(N_{0.72}C_{0.17}O_{0.11})_{1.38}$	XPS
ECR plasma [58]	$TiN_{0.74–1.07}H_{0.1–0.42}$	RBS, ERD
ECR plasma [60]	$Ti(N_{0.9–0.93}C_{0.04–0.06}O_{0.02–0.04})_{0.8–1.3}H_{0.08–0.34}$	SIMS
Low-temperature CVD [61,62]	TiN, Zr_3N_4, Hf_3N_4, $VN_{1.05–1.15}$ $NbN_{1.35}$, $TaN_{1.7}$	RBS, XPS, SAED
ThD [65]	$Zr(B_{0.67}C_{0.17}O_{0.16})_{2.25}$	AES
Implantation [68]	$TiN_{1.2}$, $ZrN_{1.5}$, $NbN_{0.9}$, $TaN_{0.8}$	RBS, XRD
DCMRS [74]	$TiN_{0.8–1.2}$	RBS, AES, XRD, EDS, SAED
DCMRS [75]	$(Ti_{0.47}Al_{0.33}Zr_{0.2})(N_{0.96}O_{0.04})_{0.96}$	EPMA, XRD
DCMRS [76]	$TiN_{0.2–1.14}$	AES
RFMNRS [77]	$TiB_{2.1–2.85}$	AES, XRD
RFMRS [78]	$Zr(N_{0.83}C_{0.13}O_{0.04})_{\sim 2}$	AES, XRD
DCMNRS [79]	$Ti(B_{0.8}O_{0.11}N_{0.045}C_{0.045})_{2.5}$	AES

Rutherford backscattering spectroscopy (RBS), elastic recoil detection (ERD), secondary ion mass spectrometry (SIMS), electron probe microanalysis (EPMA), sputtered neutral mass spectrometry (SNMS), laser induced ion mass analysis (LIMA), selected-area electron diffraction (SAED), positron annihilation spectroscopy (PAS), scanning tunnelling microscopy and atomic force microscopy (STM and AFM), etc., are being used in different combinations. These methods, providing both qualitative and quantitative determinations, have areas of overlap rather than being wholly complementary. As a rule two or three such methods are used as a minimum.

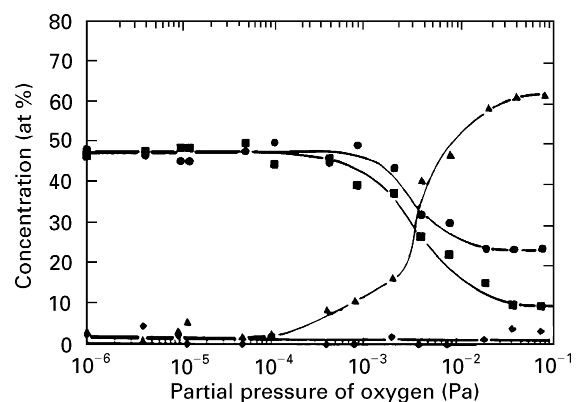

Figure 1 Surface concentrations of nitrogen and oxygen in Ti(N, O) films as a function of the O_2 partial pressure (*in situ* AES analysis) [80]. $P_{total} = 2 \times 10^{-1}$ Pa; $P_{N_2} = 2 \times 10^{-2}$ Pa. Key: ▲ O; ● Ti; ■ N; ◆ C.

3.2. Composition

Table III shows some results of IP film content analysis. In Table III and elsewhere it is supposed that N, O and C atoms are located in one sublattice (e.g. in the octahedral interstitial sites) with H atoms being in another one (e.g. in the tetragonal ones). As is evident from these results, the synthesis of an IP in a film form is frequently accompanied by the formation of superstoichiometric compounds. In conventional IP practice, this situation is not so common. Although oxygen contamination was observed to lead to the appearance of structural (nonthermal) vacancies in the metal sublattice and subsequently to superstoichiometry [2, 7].

Fig. 1 shows the variation in titanium, nitrogen and oxygen surface concentrations of the DCMRS films as a function of O_2 partial pressure [80]. The data obtained for both O_2 and H_2O impurity gases suggest that the quantity of oxygen starts to increase when the partial pressure exceeds 10^{-4} Pa (the total pressure about 2×10^{-1} Pa). Because of the high reactivity the reaction rate for O_2 and H_2O is about one order of magnitude higher than for N_2 and so the requirements of vacuum hygiene must be very high practically in all preparation methods.

It should also be noted that in many cases the availability of noble gases in the IP films is fixed. Fig. 2 shows the ratio of noble gas of Hf content as

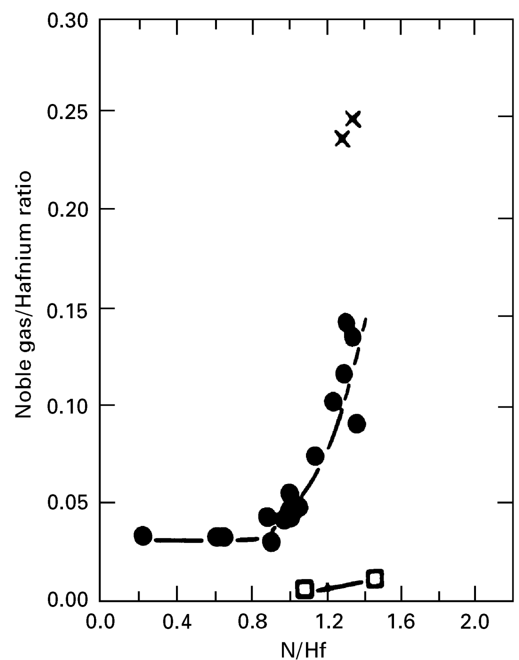

Figure 2 Noble gas/HF ratio versus N/Hf ratio in films prepared with N_2 substrate ion beam and a target beam of Ar (●), Ne (×), or Xe (□) [81].

a function of the N/Hf ratio, for films prepared by IBAD using Ar, Ne, or Xe as the target ion source (1500 eV) [81]. As is evident, the Ar content detected by RBS increases significantly when the N/Hf ratio exceeds 1.0. The content of small noble gas atoms (Ne) was even more pronounced and Xe concentration, because of the large size of its atoms, was small. In the following, a correlation of these data with electrical resistivity values will be discussed.

The interesting possibilities of XPS as applied to the phase analysis of Ti–B–N films have been demonstrated by Mollart *et al.* [82]. Fig. 3 shows the XPS B 1s and N 1s spectra for the three as deposited and annealed films obtained by RFMNRS, using composite Ti/BN targets. From these data and by assuming the presence only of the phases TiB_2, TiN and BN in the films, the phase composition of TiB_2N and $TiBN_{0.5}$ has been estimated and it was found to be in the same range as those of the phase diagram.

3.3. Structure and defects

XRD analysis, SAED, TEM, and SEM are commonly used for structure investigation of films. Such characteristics as crystallinity and amorphous state, lattice parameters, phase composition, residual stresses, microstrains, preferred orientation, dislocation structure, size and morphology of crystallites (grains) can be obtained. As applied to TiN and other IP films this topic has been described in detail elsewhere (e.g. [22, 24, 26, 83–89]). We try to concentrate attention on the most important features.

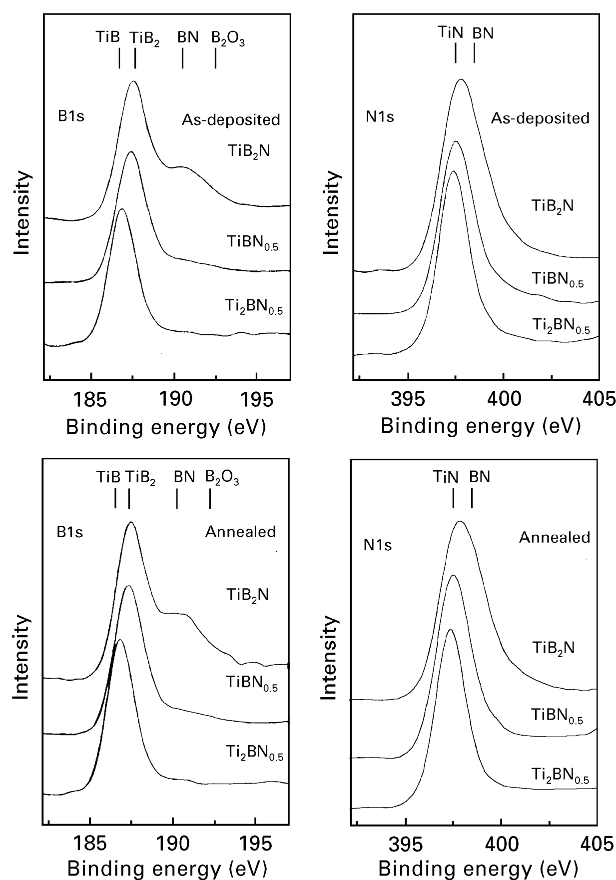

Figure 3 XPS spectra of B 1s (left) and N 1s (right) of Ti–B–N films of different composition, as-deposited and annealed at 400 °C for 280 min [82].

3.3.1. Lattice parameters and sublattice occupancy

Although this question has been studied at length, it cannot be said that unresolved features are absent. It is common knowledge that the availability of structural vacancies in the non-metallic sublattice is a characteristic feature of substoichiometric IPs [2, 7]. Conventionally this is determined by XRD and pycnometric density measurements. This is also observed in the case of nonthermal vacancies in the metal sublattice of superstoichiometric IPs. Sometimes vacancies are fixed for substoichiometric IPs with high oxygen content. However, the pycnometric density measurement as applied to films is not easy because of the small quantity of matter involved.

The decrease of TiN lattice parameter with deviation from stoichiometric content for both substoichiometric and superstoichiometric films was considered to be correct for both bulk and film specimens (e.g. [22, 87, 90]). The variation in the density of TiN with composition, as shown in Fig. 4, was also considered to be valid [22, 90]. A similar density change was also described for HfN films [91]. However, the absolute values of the lattice parameters in films are commonly larger than those in bulk specimens. This is due to the effect of high compressive stresses, substitutional and interstitial impurities such as oxygen, carbon, hydrogen, noble gases, and small grain size [22]. The quantitative role of these factors is not clear in detail. From this viewpoint the peculiarities of lattice parameter changes in IP films requires to be studied further.

It is worthy of note that lattice parameter was found to increase with decreasing film thickness and there is crystallographic anisotropy in the lattice deformation, with $a(200) > a(111)$ in substoichiometric TiN and $a(200) < a(111)$ in stoichiometric TiN [87]. The

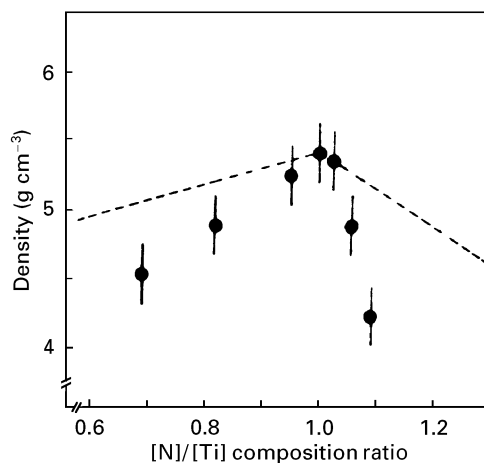

Figure 4 Film density versus composition for single-phase TiN films prepared by reactive r.f. sputtering: - - - -, theoretical density of TiN if a lack of nitrogen or titanium is compensated for by vacancies in the TiN structure [22].

latter is also observed to a greater extent for superstoichiometric TiN films and is connected with the formation of the CaF_2 phase with very small crystallites [92]. On the other hand, as indicated earlier, superstoichiometry of IPs can be connected with the formation of vacancies in the metal sublattice. The crystallographic structure for all group IVB metal superstoichiometric nitrides is found to be very close to the B1 (NaCl) structure, but with a slight rhombohedral distortion [81].

Point defects in IP films have been studied by the PAS method (e.g. [91, 93–95]). The existence of defects including vacancies, interstitials, and microvoids in these films has been determined by measuring the lifetime spectra of positrons. However, the annihilation characteristics of positrons in substoichiometric and superstoichiometric IPs are not yet fully understood. Neutron diffraction analysis seems to be necessary for revealing the localization of the different metal and non-metal atoms in the lattice, and the sublattice occupancy of nitrides and other IPs throughout their homogeneity region. Such study can be helpful for revealing the possibility of ordering vacancies as has been observed for many substoichiometric IP bulk specimens.

Some other interesting features as applied to the crystal structure of TiN, ZrN, NbN, CrN and TiB_2 films, including, for example, the dislocation loops observation, the effect of thickness on lattice parameter and NbN single-crystal deposition, have been discussed elsewhere [89, 96–100].

3.3.2. Residual stresses and texture

There are many results addressing these problems (e.g. [22, 24–26, 83, 84, 87]). The macrostrain stresses can be measured by the $\sin^2\Psi$ method and other mechanical methods. Macrostresses are thought to originate for two reasons: one is the differences in thermal expansion between the film and the substrate, and the other is a feature of film growth. Macrostresses were found to be compressive in the plane of deposition for most PVD films and the stress value was revealed to be slightly tensile for CVD TiN [25]. High compressive stresses have also been found in PVD TiC and TiB_2 films [22, 89]. It was found that the bias voltage and ion bombardment exert some action on the residual stresses (e.g. [26, 87]). The change of residual stresses in the TiN homogeneity region was found to be unmonotonous [83]. A minimum residual compressive stress was determined for $TiN_{\sim 0.7}$. It is interesting that this composition is also characterized by the maximum hardness value (see later).

The preferred orientation of CVD TiN deposition was found to be changed by the deposition temperature and the molar ratio of $TiCl_4$ to NH_3 ($m_{N/Ti}$) [86]. Three kinds of preferred orientation were determined: (1 0 0) orientation at low T_{dep}, (1 1 0) orientation at intermediate T_{dep} and low $m_{N/Ti}$, and (1 1 1) orientation at high T_{dep} and high $m_{N/Ti}$. This relationship between preferred orientation and CVD conditions is related to the change of supersaturation in the gas phase. Preferred orientation of ECR films depends also on the plasma gas; using N_2 produces the (2 0 0) orientation in TiN films, and the (1 1 1) orientation is characteristic for NH_3 [58].

For PVD $TiN_{0.88-1.0}$ the (1 1 1) preferred orientation was observed; for other compositions with low nitrogen content the (3 1 1) and (2 0 0) orientations were produced [83]. The effect of the critical thickness and the nitrogen partial pressure on the texture of TiN PVD films has been investigated in the works [101, 102]. The preferred orientation was gradually changed from (2 0 0) to (1 1 1) with increasing film thickness from 1.3 to 6.8 μm [101]. The reverse, i.e. changing from (1 1 1) to (2 0 0), is observed when the nitrogen partial pressure increases with simultaneous decreasing compressive stresses [102]. Such transformations of preferred film orientations are related to the strain energies accumulated in the films during deposition with regard to the contribution of the surface energy.

Fig. 5 shows the effect of thickness on grazing angle X-ray scans of TiB_2 films obtained by DCMRS [89]. It is obvious that the intensity ratio of (0 0 1) and (1 0 1) peaks is almost constant in films with thicknesses more than 130 nm. For thinner films (Fig. 5b) this ratio was observed to decrease, i.e. the grains are essentially randomly oriented in these films and the (0 0 1) texture starts to develop in the thicker films.

The thermal stability of IP films has been studied by numerous researchers. It was noted, for example, that annealing TiN_x films for 8 h at 500 °C causes full

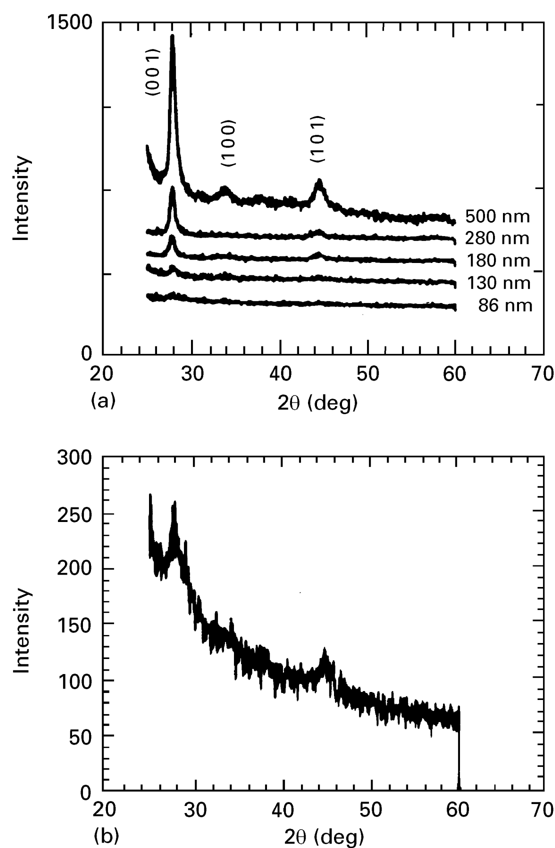

Figure 5 Grazing angle (5°) X-ray scans of TiB_2 films: (a) with different thicknesses; (b) an 86 nm thick film [89].

recovery from the preferred (1 1 1) orientation, which is one of the possible CaF_2 structures, into a randomly oriented NaCl phase structure [92]. Lowering of the compressive stress and changing the latter to a tensile one in the case of thin films (< 200 nm), has been observed in TiB_2 films after annealing at 400 °C [89]. It was also pointed out that pronounced grain growth takes place only in thinner films. Recrystallization features will be discussed later.

3.3.3. Crystallites (grains) size and morphology

The study of fine structure (crystallite size (L) and microstrains (ε)) and morphology is also very popular with regard to IP films (e.g. [22–24, 26, 84–86, 88, 97]). Fig. 6 shows the effect of the Xe^+ ion energy on the XRD pattern of a TiN film formed by IBED [103]. The broadening of peaks and changing ratio of their intensity are obvious. To estimate L, the well known Scherrer formula is often used and the full width at half-maximum (FWHM) of peaks is measured, but for a more precise determination taking into account the ε contribution in the broadening of peaks is necessary, for example, to use the Warren–Averbach method. Table IV shows some results of L and ε determinations in IP films. As is evident L is equal to or lower than 50 nm in most cases and these films really have nanocrystalline structure.

The effect of substrate temperature, bias voltage, and sputtering time on the value of L determined from TiN (1 1 1) diffraction line has been investigated by Maheo and Poitevin in detail [106]. It is interesting that when the bias voltage is − 100 or − 200 V, L lies in the region of 25 nm and the substrate temperature effect in the region of 200–500 °C is absent. With zero bias voltage the crystallites have a size about

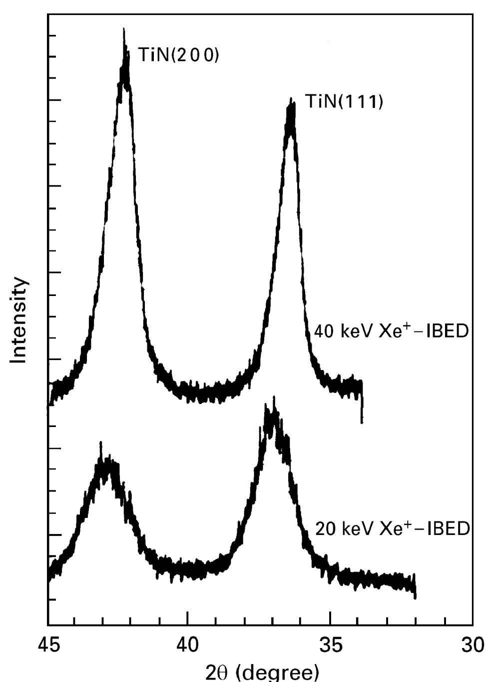

Figure 6 XRD spectra of X^+-IBED TiN film on (1 0 0) Si [103].

TABLE IV Crystallite size (L) and microstrain (ε) values obtained from XRD analysis ((1), using Scherrer formula; (2), accounting for the ε contribution)

Phase	Preparation conditions	L(nm)	$\varepsilon \times 10^3$
$TiN_{0.48-1.0}$ [83]	CAPD	9–21 (2)	0.8–2.6 (2)
TiN [88]	IBED	4–8 (1)	
Ti_2N [88]	IBED	6–21 (1)	
ZrN [97]	RFMRS		9 (2)
TiN [103]	IBED	5–20 (1)	
TiN [104]	Electron shower	35 (1)	
	CAPD	20 (1)	
	DCMRS	35 (1)	
TiN [105]	DCMRS	23–66 (2)	0.8–13 (2)
TiN [106]	DCMRS	30–140 (1)	
NbC [107]	DCMNRS	~6 (1)	

50 nm, when the temperature is low (< 400 °C), and about 70 nm at $T > 500$ °C. Large variations were observed when the bias voltage was − 60 V; in this case the distinct increase of crystallite growth (up to = 100–140 nm) was observed; crystallite growth was unmonotonous at small times. These results are closely connected with the peculiarities of ion bombardment, admixture behaviour, and adatom mobility. Note also that it is not only XRD analysis that gives relevant information on size structure. It is well known that XRD analysis gives information on the dimension of the coherently diffracting domains which are usually smaller than the grain and columnar sizes TEM (bright and dark field observations) and SEM including the HR version are generally used for full structure characterization and their results are more comprehensive than XRD in most cases (e.g. [56, 83, 106]). Although the agreement between TEM and XRD results is also shown as in the case of NbC film [107]. The discrepancy between the different methods of the L determinations as applied to nanocrystalline materials has been discussed elsewhere [108].

TEM analysis and XRD data provide a means for obtaining information about superlattice or multilayer thin films (uniformity of layer thickness, composition modulation, and interface roughness) [84]. Dislocation structure in these subjects was also investigated by TEM [85]. Edge misfit dislocations with the Burgers vector $\frac{1}{2}\langle 1\,1\,0\rangle$, which are characteristic for the NaCl-structure transition metal carbides and nitrides, were found in all investigated superlattice films of TiN, NbN, VN, and TiVN which were deposited by DCMRS on a MgO (1 0 0) substrate. Strain relaxation is determined by the effect of lattice mismatch and film thickness. The dislocation loop density in epitaxial TiN (1 0 0) films, deposited by DCMRS onto MgO (1 0 0) substrate, has been found to decrease from 5×10^{12} to 1.5×10^{10} cm^{-2} as substrate temperature increased from 550 to 850 °C [99].

The IP film microstructure can be represented by columnar and equiaxied particle morphologies with various intermediate cases of the two. Fig. 7 shows a typical fully dense columnar structure of a TiN film, obtained by RFMRS, after load indentation [109].

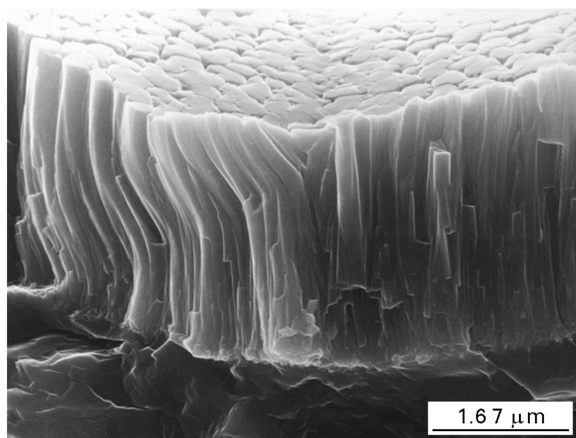

Figure 7 High resolution SEM image of a fractured cross-section of TiN film by indentation imprint (courtesy of Ma and Bloyce [109]).

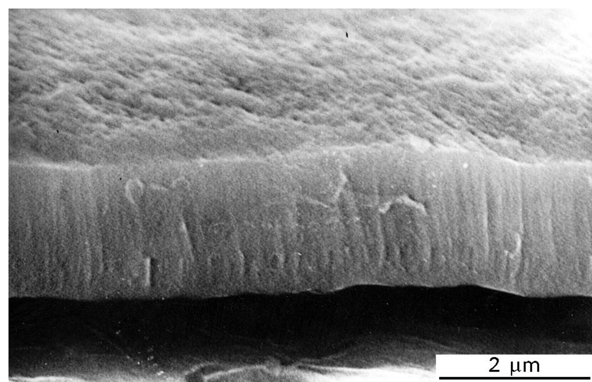

Figure 8 SEM image of a fractured cross-section of TiB_2 film obtained DCMNRS [112].

The example of plastic deformation of brittle TiN is very impressive. As is evident in this picture, the width of the columns is about 200–300 nm. The effect of the substrate temperature and bias voltage on the columnar morphology of the TiN film has been studied in [106]. It was stressed that the top of each column looked like a triangular or square section of a pyramid and the width of the columns changed with temperature and bias voltage from 50 to 500 nm. These values are higher than those obtained from the half-height width of the TiN (1 1 1) diffraction line (see Table IV). This difference may be caused by the approximate value of L obtained by using only the Scherrer relationship. Another type of TiN film structure, the glassy, non-columnar one, has been observed using DCMRS (four unbalanced rectangular planar magnetrons incorporated saturated ferrite magnets with a bias voltage of -100 V) [110]. At the same time using neodymium–iron–boron magnets in the magnetrons gives a bias voltage of only -40 V and results in film with a columnar structure.

SEM study of TiB_2 and $Ti(B, N)_x$ films has revealed different kinds of structure (e.g. [77, 79, 111, 112]). A stone-like or cauliflower-like structure with a partly columnar one are typical for these films (Figs 8 and 9), with the latter largely obtained in the nitrogen containing films. The surface topography of films can be also studied by SEM [112] and especially using STM and AFM (e.g. [113]).

The grain size of TiN films obtained by conventional CVD can be regulated by deposition with and without interrupted growth as well as by using dopants (e.g. $AlCl_3$) during the process [27]. CVD TiN films obtained from organometallic precursors at low temperatures are characterized by an ultrafine granular structure with poorly defined grain boundaries [61]. On the other hand, in the case of CVD co-deposition, such as SiC–TiC–C composite [114], nano L sizes about 10–20 nm along the $\langle 2\,2\,0\rangle$ direction have been obtained above 1000 °C. Defects in coating as a whole have been analysed by Babad-Zakhriapin [115] in connection with the growth peculiarities.

As is evident from the foregoing a wide variety of different morphology structure types is observed for

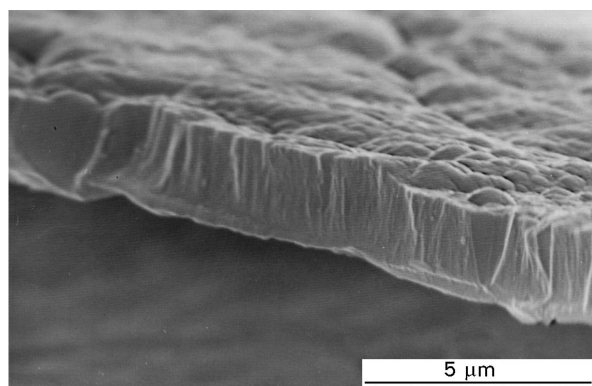

Figure 9 SEM image of a fractured cross-section of $Ti(B, N)_x$ film obtained by DCMNRS [112].

IP films as a result of temperature, substrates, admixtures, ions characteristics, and other factor effects in different CVD and PVD processing. Hence, all these versions seem to be unlikely to reduce to the growth models of Movchan and Demchishin [116] as well as Tornton [117] and the need for further investigation is needed (see also review [26]).

3.4. Bonding

The XPS method is often used for film characterization (see Table III and Fig. 3) and for revealing the peculiarities of their electron structure (e.g. [21, 61, 62, 93, 118–120]). The Ti $2p_{3/2}$, B 1s and N 1s core level binding energies for $Ti(B, N)_x$, TiB_2 and TiN coatings as well as the Ti 2p, N 1s and O 1s for TiN_x and TiN_xO_y films have been studied [82, 118, 119]. The effective charges of Ti, O and N atoms in films have been estimated [119]. However, it was stressed that the results obtained were preliminary. The effect of lattice defects on the core level binding energies in XPS spectra and some difficulties in understanding the nature of nitride films have been discussed by Perry [93]. Some experimentally obtained binding energies of nitride films, prepared using an organometallic precursor and ammonia at low temperature, are presented in Table V.

These films were characterized by a very low admixture content (less than 1–2 at % oxygen and carbon)

TABLE V XPS binding energies (eV) for films deposited on silicon at 200 °C [61, 62]

Film	Precursors	N 1s binding energy	Metal line	Binding energy
TiN	$Ti(NMe_2)_4/NH_3$	396.9	Ti $2p_{3/2}$	454.8
Zr_3N_4	$Zr(NMe_2)_4/NH_3$	397.2	Zr $3d_{5/2}$	180.3
Hf_3N_4	$Hf(NMe_2)_4/NH_3$	397.0	Hf $4f_{7/2}$	15.1
VN	$V(NMe_2)_4/NH_3$	397.0	V $2p_{3/2}$	513.1
Nb_3N_4	$Nb(NEt_2)_4/NH_3$	397.4	Nb $3d_{5/2}$	204.1
Nb_3N_4	$Nb(NMe_2)_5/NH_3$	397.2	Nb $3d_{5/2}$	203.9
Ta_3N_5	$Ta(NMe_2)_5/NH_3$	396.9	Ta $4f_{7/2}$	24.0

and have an ultrafine granular structure (2–5 nm and smaller). However, the hydrogen content was in the range 0.5–1.35 hydrogen-to-metal ratio. From the discussion of the results of Table V [61, 62], in most cases these binding energy values are typical for transition metal nitrides. The difference in XPS data for conducting ZrN and insulating Zr_3N_4 has been pointed out elsewhere [120].

4. Properties

4.1. General characteristics

As will be clear from the following, only electrical and optical properties as well as hardness of IP films have been investigated in detail. This is not accidental because their main application areas are microelectronics and optical devices, wear-resistant and protective coatings on cutting tools and mechanical parts, and for decorative purposes such as surface-finishing paints. Information on other properties is not so comprehensive.

TABLE VI Some data of room-temperature electrical resistivity (ρ) values for IP films

Phase	Preparation method	ρ(μΩ cm)
$Ti_{\sim 2}N$ [22]	DCMRS	~200
$Ti(N_{0.72}C_{0.17}O_{0.11})_{1.38}$ [57]	ECR plasma	~250
$Ti(N_{0.68}C_{0.22}O_{0.10})_{1.44}$ [57]	ECR plasma	~600
$TiN_{0.86}$ [58]	ECR plasma	45
$TiN_{1.02}H_{0.15}$ [58]	ECR plasma	100
$TiN_{\sim 1.2}$ [74]	DCMRS	120
$TiN_{1.06}$ [76]	ARE	82
$TiN_{\sim 1.0}$ [121]	DCMRS (single-crystal film)	18
$TiN_{\sim 1.0}$ [122]	CAPD (filtered version)	20
Zr_3N_4 [61]	CVD (T = 200–400 °C)	> 10^6
ZrN_x [76]	ARE	112–255
$ZrN_{\sim 1.2}$ [78]	RFMRS	~100
$ZrN_{\sim 1.0}$ [123]	IBAD	17.8
Hf_3N_4 [61]	CVD (T = 200–400 °C)	> 10^6
HfN_x [124]	RFMRS	~200
VN_x [62]	CVD (T = 200 °C)	~10^3
Nb_3N_4 [62]	CVD (T = 200 °C)	10^3–10^4
NbN [98]	IBAD + ECR plasma	75
$Ta_{\sim 2}N$ [125]	RFMRS	200
Ta_3N_5 [62]	CVD (T = 200 °C)	> 10^6
$MoN_{\sim 1.0}$ [126]	DCMRS	~480
$W_{\sim 2}N$ [126]	DCMRS	~400
$WN_{\sim 0.9}$ [127]	RFMRS	~450
$TiC_{\sim 1.0}$ [128]	ARE	40
$TiC_{0.8}$ [128]	CVD	196
$ZrC_{0.9}$ [128]	ARE	560
$NbC_{0.98}$ [37]	LRS	20–50
$NbC_{\sim 1.0}$ [129]	LRS	4 (T = 13 K)
$TiB_{\sim 2}$ [130]	RFMNRS	500 (150)
$TiB_{1-2.1}$ [131]	DCMNRS	~260 (120)
$ZrB_{\sim 2}$ [130]	RFMNRS	250 (75)
HfB_x [132]	Co-r.f.sputtering B and Hf	~370
$YB_{\sim 2}$ [133]	Dual EBE	55
$YB_{\sim 4}$ [133]	Dual EBE	51
$YB_{\sim 6}$ [133]	Dual EBE	88
$LaB_{\sim 6}$ [133]	DCMNRS	104
$TaH_{0.48}$ [134]	EBE and hydriding	~46

4.2. Electrical and optical properties

To our knowledge these properties in general as applied to TiN films have been considered only in review [22]. It is a matter of familiar experience that the vast majority of IPs are metallic conductors and their electrical resistivity (ρ) increases with increasing temperature. In many cases the ρ value of a stoichiometric IP is lower in comparison with those for corresponding metals such as for borides, nitrides and hydrides of the group IVB transition metals (e.g. [2, 7, 18]). This is related to their electron structure and in particular to the high mobility of carriers. At the same time a number of superstoichiometric IPs behave as semiconductors and dielectrics. It should be also pointed out that the effect of admixtures and structural vacancies on the ρ value is very sensitive for an IP. This situation, added with complexity of the influence of strain state, grain size and thickness, takes place in the case of IP films. Table VI shows some ρ values.

Table VI does not include all results but only those which have adequate characterization. Here, too, the information of all admixture contents cannot be overestimated. So the analysis and comparison of these results must be done with some reservation. Nevertheless it is possible to point out that the ρ change is not monotonous in the homogeneity region of IP films. Fig. 10 shows this statement very visually as applied to the group IVB metal nitrides [81]. The deviation from stoichiometry results in ρ increasing at the cost of scattering of the conduction electrons on structural vacancies in the case of substoichiometric IP. On the other hand, superstoichiometric nitrides, especially $ZrN_{>1}$ and $HfN_{>1}$, convert to insulating phases with N content increases. This conversion for the composition Me_3N_4 was predicted by electron energy calculations [135]. As indicated above, the formation of these compounds in the powder form is not often observed and this may be possible in the presence of noble gases (see Fig. 2) and oxygen. Another type of ρ change, namely, the decrease with deviation from stoichiometry has been shown in WN_x films [127].

It is worth noting that the resistivity ratio ρ(300 K)/ρ(20 K) for superconducting NbN films was only 1.7 (T_c = 8.6 K) [98]. This ratio (T = 13 K) for NbC films was about 3 (T_c = 12 K) [37]. Evidently the resistivity

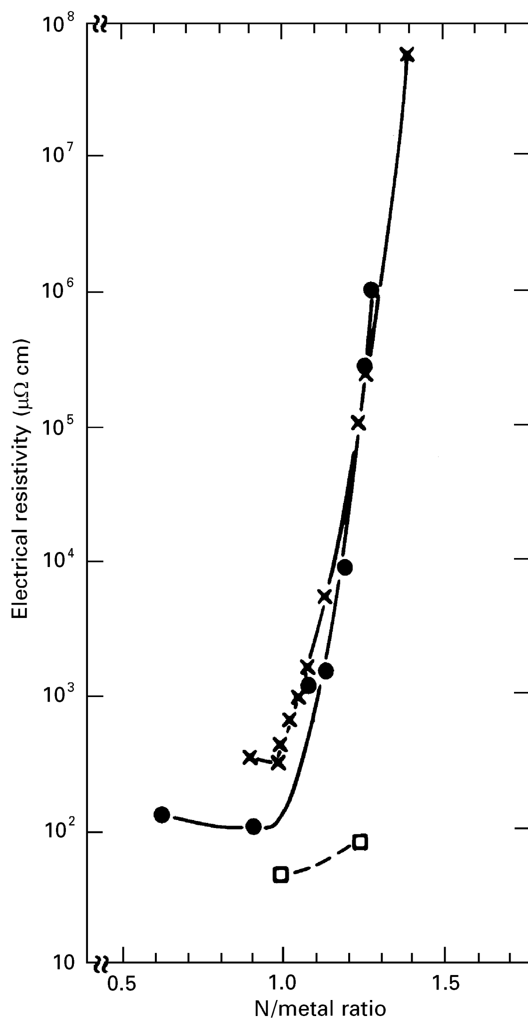

Figure 10 Electrical resistivity versus N/metal ratio in films of Hf–N (●), Zr–N (×), and Ti–N (□) [81].

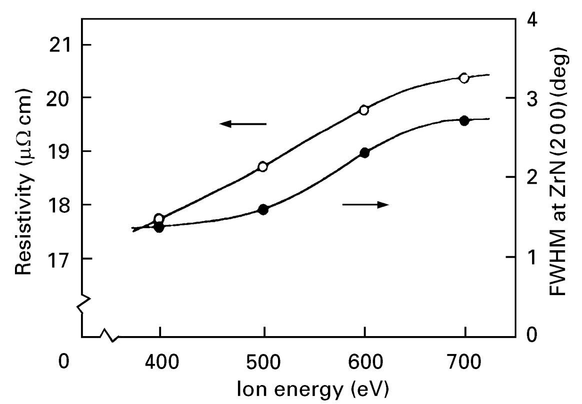

Figure 11 Ion-energy dependencies of the resistivity (○) and the full width at half-maximum (●) at the ZrN (200) peak [123]. The arrival rate ratio is the ratio between N and Zr fluxes arriving at the substrate. Substrate temperature = 820 °C. Arrival rate ratio N/Zr = 1.5.

ratio and T_c values for NbN are not very high. This is due to both the impurities and thickness effect (the thickness value for NbN was 30 nm and for NbC was 10–800 nm). Ritala *et al.* [63] pointed out that TiN films deposited by CVD at 500 °C with zinc obtained a minimum ρ value (about 50 μΩ cm) only in the case of thicknesses above 100–150 nm. It is also characteristic that the lowest value of ρ in Table VI (17.8 μΩ cm) was obtained for $ZrN_{\sim 1.0}$ film prepared at high substrate temperatures and low ion energy, which favoured the improvement of the crystalline quality as is shown from Fig. 11 [123]. Deposition of single-crystal TiN film on (1 1 1) MgO substrate at a temperature of about 800 °C was also found to lead to a low ρ value (18 μΩ cm); ultrapure (99.9999%) gases were used [121]. The ρ values after annealing are indicated in brackets for TiB_2 and ZrB_2 (as well as for rare earth borides). It is interesting that for HfB_x films an increase in the x value from 1 to 5 was shown to increase the film resistivity by less than a factor of 2, but an increase in the oxygen impurity content from 0.3% to 0.6% was found to increase the ρ value by about an order of magnitude.

As is evident from Table VI the ρ values spectrum is very wide and in many cases the absence of information on impurity content, thickness value, and crystal size makes a comprehensive discussion difficult. The limited data for hydride films have engaged our attention although in recent times these investigations as applied to intermetallic hydrides such as $FeTiH_x$, $LaNi_5H_x$ and $LaCo_5H_x$ are being enlarged (e.g. [136–138]). However, as a rule the absolute ρ values and hydride compositions are not reported.

The temperature coefficient of resistivity (TCR) gives important information about the type of scattering and the role of impurities and crystallites or surfaces. Table VII summarized the data of effect of TiN different deposition conditions on ρ, T_c, δT and TCR [139].

The great influence that film preparation conditions have on electrical properties is evident. It was pointed out that the optimal condition to deposit the lowest ρ value of a TiN film also gives the highest TCR. Increasing the film thickness up to 264 nm results in an increase of TCR to a value of 6356 p.p.m. K^{-1}, which compares favourably to 6200 p.p.m. K^{-1} reported for a single crystal (1–2 μm thick) [121]. As Sundgren [22] has noted, for stoichiometric TiN polycrystalline films the TCR value is between 1000 and 2000 p.p.m. K^{-1}. A negative TCR is typical for solids with a non-metallic conduction mechanism such as Zr_3N_4 [78] and possibly NbN [140]. Although in the latter case the profound effect of grain structure on TCR is also considered [98].

A detailed study of the electronic properties of epitaxial TiN/VN (0 0 1) superlattices was performed by Hirashita *et al.* [141]. Hall and ρ measurements carried out as a function of the superlattice period (Λ) revealed that electron carrier concentration (n) was constant at 4.5×10^{22} cm^{-3} while ρ increased and the electron mobility (μ) as well as a positive TCR decreased rapidly with $\Lambda < 6$ nm. For very thick layers ($\Lambda \geqslant 10$–15 nm) the following values have been obtained: $\rho \sim 30$ μΩ cm, $\mu \sim 5$ $cm^2 V^{-1} s^{-1}$, TCR ~ 1600 p.p.m. K^{-1}. The estimated value of the room-temperature electron mean free path (λ) using the Drude model and assuming a spherical Fermi surface was about 4.6 nm for TiN and was the same for VN. These estimations were considered to be approximate because the Fermi surfaces of nitrides are known to be

TABLE VII Room-temperature electrical resistivity (ρ), the temperature coefficient of resistance (TCR), superconducting transition temperature (T_c), and superconducting transition width (δT) for TiN films reactively sputtered onto thermal SiO_2. The thin film thickness is between 30 and 100 nm [139]

Substrate T(C°)	r.f. bias (− V)	ρ (μΩ cm)	TCR (p.p.m. K^{-1})	T_c (K)	δT
40	0	205–215	264	< 4.3	0.04
40	115	120–135	561	< 4.3	0.04
500	0	65–70	1018	4.84	< 0.02
500	100	45–60	1335	5.04	< 0.02

anisotropic. None the less, these estimations seem to be likely bearing in mind the layers thickness (e.g. $\Lambda \sim 6$ nm, $l \sim 3$ nm). Note that λ_{TiN} estimations conducted by Tsai *et al.* [139] revealed the highest values, $\lambda_{TiN} = 39$–96 nm (these correspond to data in Table VII). For a near stoichiometric NbC film the λ value was more than 40 nm [129]; the second critical field in this case was 7 kOe and the density of electronic states at the Fermi level was 1.3 states/eV-atom Nb. Unfortunately, information on electronic properties, such as the Hall coefficient, thermoelectric power, magnetoresistance, etc., is very limited for IP films. To our knowledge only some data for TiN [121, 142], HfN [124], and $FeTiH_x$ [138] films are available.

The optical properties of films are important in decorative and solar applications. They have been discussed with respect to the IVB nitrides and especially to TiN in reviews [22, 93]. It is common knowledge that $TiN_{\sim 0.5}$ specimens are metallic grey, $TiN_{\sim 0.8}$ are clear yellow, $TiN_{0.95-0.97}$ are golden yellow and $TiN_{>1.0}$ are brown. This behaviour results from the peculiarities of electron structure in the TiN homogeneity region and is analysed in [22, 93].

The optical properties and colour are controlled by the process and deposition parameters such as nitrogen partial pressure, substrate temperature, bias voltage, etc. Eventually, as in the case of many other properties, variation in stoichiometry, purity and surface morphology are mainly responsible. A maximum value of reflectance of about 0.95 is characteristic for TiN films in the near infrared region. In the ultraviolet, a minimal value of reflectance reaches about 0.1. Table VIII shows some selected optical properties of nitride films.

Examples of the impurities and surface roughness effect can be found elsewhere [61, 144]. The refractive indices were 2.15–2.25 for zirconium nitride films containing 10 at % oxygen [61]. Bonelli *et al.* [144] have shown that the spectral reflectivity at 220 nm decreases from 40 to 27% for sputtered TiN films, whereas for TiN films prepared by the filtered arc method, the decrease in reflectivity was from 29 to 16%.

Optical properties of TiN_xO_y films obtained by DCMRS on architectural glass have been studied by Polato *et al.* [145]. The plasma energy of TiN_x, obtained from *in situ* spectroscopic ellipsometry experiments, was found to depend strongly on the

TABLE VIII Selected optical properties

Film	Optical band gap (eV)	Refractive index*	Reflectivity (%) (phot.energy = 2.8 eV)
Zr_3N_4 [61]	2.2	2.9–3.3	
Hf_3N_4 [61]	2.7	2.4–2.8	
VN [62]		1.5–1.7	
Nb_3N_4 [62]		2.5–2.9	
Ta_3N_5 [62]	2.7	3.0–3.1	
$TiN_{\sim 1.0}$ [63]			0.13
$TiN_{\sim 1.0}$ [76]			0.20
$TiN_{0.67}$ [76]			0.45
$TiN_{1.04}$ [143]			0.1
$ZrN_{\sim 1.0}$ [76]			0.20

*Film refractive indices were measured by using a fixed-wavelength (622.8 nm) ellipsometer.

deviation of the stoichiometry [146]. This value can be used as a parameter for *in situ* monitoring of TiN_x stoichiometry.

4.3. Hardness and elastic properties

Undoubtedly hardness measurements are most popular for film characterization because of the ease of realization and the usefulness of the information obtained. However, in some cases the interpretation of these results is not so easy with respect to the known high structural sensitivity of hardness and its dependence on load as well as the test method used. The effect of film thickness and substrate type, not to mention the influence of contamination, must also be considered. Sometimes the absolute hardness values are not comparable or at least demand detailed consideration. When applied to IP films, the hardness problem has been repeatedly discussed (e.g. [22–27, 79, 83, 84, 112, 121, 122, 147–151]).

Let us consider this question given, as an example well studied TiN films. The effect of different factors on hardness are shown in Figs 12–15. As mentioned above, the authors [83, 121, 122] have paid much attention to film preparation and their characterization. It is easy to show that the results shown in Figs 12 and 13 fit to the Hall–Petch relationship between hardness (strength) value and crystallite size. However, not only can L value affect hardness, as is evident from Fig. 14, but the N content and residual compressive stresses were not constant in these specimens and Figs 12 and 13 reflect the combined effects. For bulk TiN specimens the hardness increase with decreasing N content in the homogeneity region has been determined recently with confidence [17, 90] in contrast to old data (e.g. [23]). It is also important that Figs 12 and 13 are characteristic for different load intervals covering both nanoindentation testing and conventional Vickers hardness because of the load effect that takes place (Fig. 15). At the same time it should be recorded that some results [83, 122] are in rather poor agreement both with the given data set and (for example, the effect of residual stresses on hardness is opposite) with some other data [87]. Possibly these

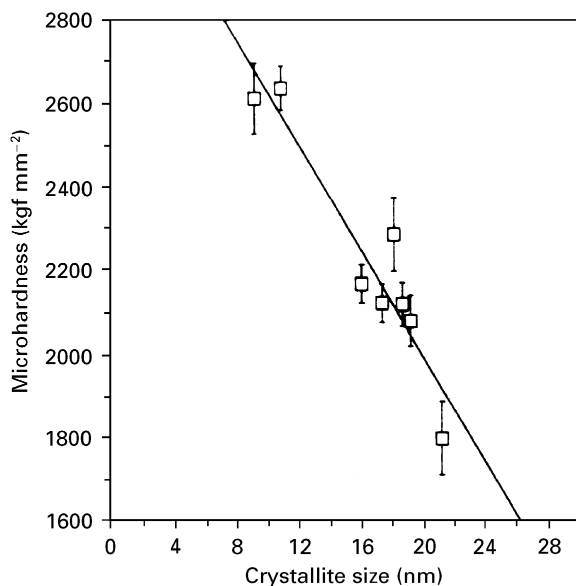

Figure 12 The variation in microhardness of TiN films with crystallite size [83]. The load was 1N; the film thickness varied from 20 to 25 μm; films were deposited by filtered CAPD on a Ti–6Al–4V alloy substrate.

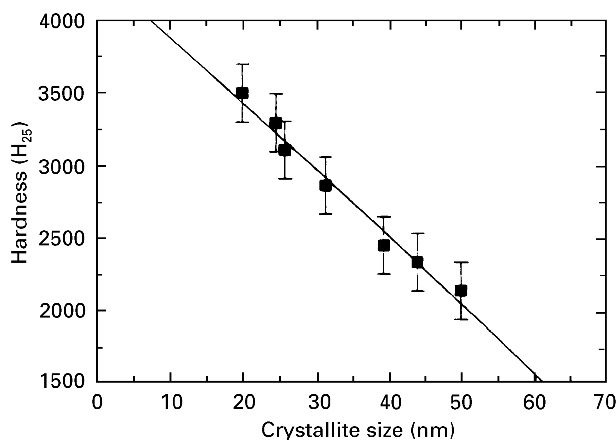

Figure 13 The same as in Fig. 12 with nanoindentation testing [122]. The load was 25 mN; the film thickness was 1–5 μm; films were deposited by filtered CAPD on a stainless steel (SUS 316) substrate.

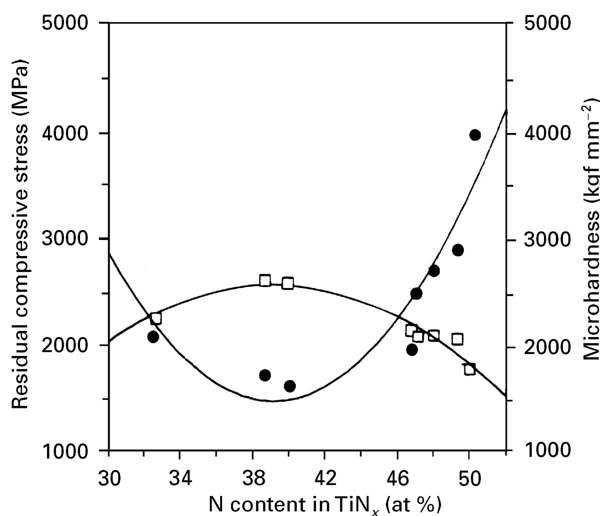

Figure 14 Microhardness (□) and residual compressive stress (●) of TiN_x films as a function of N content [83].

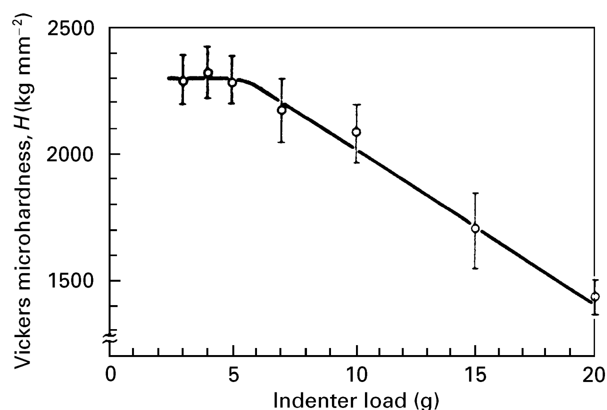

Figure 15 Microhardness of single-crystal (1 1 1) TiN film as a function of indenter load [121]. The film thickness was of 2 μm; the films were deposited by DCMRS on (1 1 1) MgO substrate at temperature $T_s = 800\,^{\circ}C$.

differences are due to unequal thickness values and substrate types (see comments in legends to Figs 12 and 13). Furthermore the method of L determination in films was also different, e.g. the Warren–Averbach method [83] and the FWHM of broadened (1 1 1) diffraction lines [122]. The uncertainty in L determinations was mentioned early in Section 3.3.3.

From the above it is seen that the situation with hardness interpretation is not so simple even in the case of very well characterized specimens with low ρ values (see Table VI). It is possible to agree with the opinion of Soderlund and Rowcliffe [152] who pointed out that "in spite of its popularity indentation hardness is ill-defined as a materials parameter". Nevertheless Table IX summarizes data for the hardness values of IP films with the accent on the most relevant information.

The hardness values of Table IX in round brackets relate to estimated values [79, 157, 173] using the Jonsson and Hogmark relationship [147] based on an "area law of mixtures". Such modelling of thin film hardness as hardness of composite (film and substrate) tends to give the hardness of films themselves or proper hardness. In many cases Knoop and Vickers test results do not coincide; sometimes the Knoop values are lower than the Vickers ones. Apart from our comments on Figs 12–15, the effect of load, deviations from stoichiometry and crystallite (grains) size, on the results given in Table IX, the following considerations are also noteworthy.

1. The regimes and methods of deposition exert deep action on the hardness values especially substrate temperature, bias voltage and annealing temperature (e.g. [79, 121, 122, 157, 160, 165, 175]). All these parameters actively influence the film structure. In this connection a very interesting example has been demonstrated by Holleck and Lahres [165] in the case of TiC/TiB_2 films, deposited by DCMNRS and studied in the as-deposited (amorphous) and annealed (crystalline) states. It is notable that while hardness of amorphous TiC and TiB_2 was lower than that for crystalline ones, the

TABLE IX Vickers microhardness of some IP films

Phase	Preparation method	Thickness (μm)	Load (N)	Substrate	Hardness (GPa)
$TiN_{1.0}$ [83]	CAPD (filtered)	20–25	1	Ti–6Al–4V	17.6 ± 0.9
$TiN_{0.92}$ [83]	CAPD (filtered)	20–25	1	Ti–6Al–4V	20.8 ± 0.5
$TiN_{0.87}$ [83]	CAPD (filtered)	20–25	1	Ti–6Al–4V	21.2 ± 0.45
$TiN_{0.66}$ [83]	CAPD (filtered)	20–25	1	Ti–6Al–4V	25.6 ± 0.8
$TiN_{0.48}$ [83]	CAPD (filtered)	20–25	1	Ti–6Al–4V	22.4 ± 0.85
TiN_x [109]	RFMRS	1.8–4.5	0.1	M2 steel	~34.3
TiN_x [110]	RFMRS	4.8	0.15	M2 steel	~31.2 (Knoop)
(1 1 1) $TiN_{\sim 1.0}$ [121]	DCMRS	2	0.03–0.05	(1 1 1) MgO	22.6 ± 0.2
$TiN_{\sim 1.0}$ [122]	CAPD (filtered)	1.0–1.5	0.025	SUS 316	34.4
$TiN_{1.0}$ [153]	DCMRS	5	0.01–0.03	SUS 304	~24
$TiN_{0.96}$ [153]	DCMRS	5	0.01–0.03	SUS 304	~30
$TiN_{0.86}$ [153]	DCMRS	5	0.01–0.03	SUS 304	~28
$TiN_{0.75}$ [153]	DCMRS	5	0.01–0.03	SUS 304	24–29
$TiN_{0.55}$ [153]	DCMRS	5	0.01–0.03	SUS 304	31–32
$TiN_{1.53}$ [154]	IBAD (reactive)	0.3	0.25	SUS 304	~30
$TiN_{1.19}$ [154]	IBAD (reactive)	0.3	0.25	SUS 304	~35.2
$TiN_{0.9}$ [154]	IBAD (reactive)	0.3	0.25	SUS 304	~35
$TiN_{0.47}$ [154]	IBAD (reactive)	0.3	0.25	SUS 304	~27.3
$TiN_{0.95}$ [155]	PVD ($T = 500\,^{\circ}C$)	5	0.025	WC/Co	32.4 ± 3.7
ZrN_x [156]	CAPD	2–3	0.5	SUS 304	26–32 (Knoop)
ZrN_x [157]	CAPD	2	0.5	WC/Co	27 ± 2
HfN_x [156]	CAPD	2–3	0.5	SUS 304	26–32 (Knoop)
(1 0 0) VN_x [158]	DCMRS	2.5	0.08	(100) MgO	$\sim 15.9 \pm 0.2$
NbN_x [157]	CAPD	2	0.5	WC/Co	34 ± 2
CrN_x [157]	CAPD	2	0.5	WC/Co	23 ± 2
(1 0 0) $(Ti_{0.5}V_{0.5})\ N_x$ [158]	DCMRS	2.5	0.08	(100) MgO	20 ± 0.27
$(Ti_{0.5}V_{0.5})\ N_x$ [159]	CAPD	~5	0.5	HSS	~32
$(Ti_{0.25}V_{0.75})\ N_x$ [159]	CAPD	~5	0.5	HSS	~44
$Ti_{0.5}Al_{0.5}\ N_x$ [160]	DCMRS	3	0.1	SUS 321	41 ± 9.8
$Ti_{0.7}Zr_{0.3}\ N_x$ [161]	DCMRS	5	0.5	WC/Co	~33
(Ti,Al,Zr) N* [75]	DCMRS	5	0.5	WC/Co	34.3
TiC_x [155]	CVD	6.5	0.025	WC/Co	38.9 ± 6.0
TiC_x [162]	CAPD ($T = 700\,^{\circ}C$)	5–7	0.5	HSS	39.3
	($T = 600\,^{\circ}C$)	5–7	0.5	HSS	36.2
$TiC_{\sim 0.85}$ [163]	PACVD ($T = 700\,^{\circ}C$)	15	0.5	WC/Co	~39
$Ti(C_{\sim 0.86}O_{\sim 0.14})$-$C_{\sim 1.04}$ [164]	IBAD	1.5	0.1	(1 1 1) Si	28.2 (Knoop)
TiC_x [165]	DCMNRS	5	0.5	WC/Co	33.3
TiC_x [165] (amorphous)	DCMNRS	5	0.5	WC/Co	24.5
$TaC_{\sim 1.0}$ [166]	CVD ($T = 800\,^{\circ}C$)	8	0.5–3.9	Ta	(14.6)
$W(C_{0.93}O_{0.07})_{1.12\text{–}1.18}$ [167]	RFMRS	7	0.01	SUS 304	31
WC_x [168]	RFMRS	5	0.15	HSS	45.5
TiCN [155]	CVD	3	0.025	WC/Co	30.8 ± 3.1
$TiC_{0.5}N_{0.5}$ [162]	CAPD ($T = 600\,^{\circ}C$)	5–7	0.5	HSS	26
$TiC_{0.2}N_{0.8}$ [162]	CAPD ($T = 600\,^{\circ}C$)	5–7	0.5	HSS	26
$(Ti_{0.7}Zr_{0.3})\ C_x$ [161]	DCMRS	5	0.5	WC/Co	45
$TiB_{\sim 2}$ [169]	DCMNRS	5	0.5	WC/Co	34
$TiB_{\sim 2}$ (amorph.) [165]	DCMNRS	5	0.5	WC/Co	23.5
$TiB_{\sim 2.8}$ [170]	DCMNRS	4.1	0.15–0.30	WC/Co	51
$TiB_{\sim 2}$ [171]	RFMNRS	5	0.25	Cr steel	37.2
$TiB_{\sim 1.9}$ [172]	DCMNRS	~8	0.5	HSS	~62.5
$TiB_{\sim 2}$ [173]	Dynamic ion mixing	1	0.25–0.75	WC/Co	(27.5)
$Ti(B, O, N, C)^{*}_{2,5}$ [79]	DCMNRS	1.8	0.5	(1 0 0) TiB_2	44.7 ± 4 (50–52)
$ZrB_{\sim 2}$ [174]	DCMNRS	5	0.2	CrNiMo steel	21.6
$TiB_{1.6}N_{0.6}$ [170]	DCMRS	4.9	0.15–0.3	WC/Co	57
$TiB_{\sim 2.1}N_{\sim 0.6}$ [172]	DCMRS	5	0.5	HSS	41.5
$TiBN_{0.4}$ [175]	RFMNRS ($T = 20\,^{\circ}C$)	1–3	($\delta = 100$ nm)	HSS	~30
	($T = 400\,^{\circ}C$)	1–3	($\delta = 100$ nm)	HSS	55
$TiB_{1.8}C_{0.5}$ [170]	DCMRS	2.7	0.15–0.3	WC/Co	43
$TiB_2C_{0.4}N_{0.4}$ [170]	DCMRS	4.9	0.15–0.3	WC/Co	50

* See the detailed compositions in Table III.

opposite occurred for mixed annealed and crystalline compositions (TiC/TiB_2) deposited from a 50/50 target. A hardness increase of $Ti(B,N)_x$ films of ~2 times as a result of increase of temperature deposition from 20 to 400 °C was also observed by Hammer *et al.* [175].

2. Note also that, as a rule, CAPD regimes tend to higher hardness values as compared with other methods. So in the case of Ti_2N_x and TiN_x at optimum nitrogen pressure and substrate temperature values of ~46.5 and ~42 GPa (load was of 0.5 N; thickness was of 4–6 μm) have been

obtained, respectively. However nitrogen content in these films was not determined [176, 177]. The effect of nitrogen pressure on hardness, lattice parameter and the FWHM of peaks in the case of Ti–N, Ti–Zr–N, Zr–N, and Ti–Mo–N films deposited by CAPD is shown in Fig. 16 [177]. Maximum values of H_v were observed for deposition conditions when phase composition was Ti_2N_x and TiN_x and the FWHM values achieve their maximum. Characteristically, the H_v maximum for the cubic phase is in the substoichiometric range because the lattice period of the stoichiometric structure is achieved with higher nitrogen pressures (Fig. 16a). Introduction of metal additions up to 50 wt % does not induce qualitative changes in the aforementioned features (Fig. 16b and c). However, when the Zr content is increased by more than 50 wt % we observe only one maximum for the cubic phase (Fig. 16d and e) which is connected with the absence of

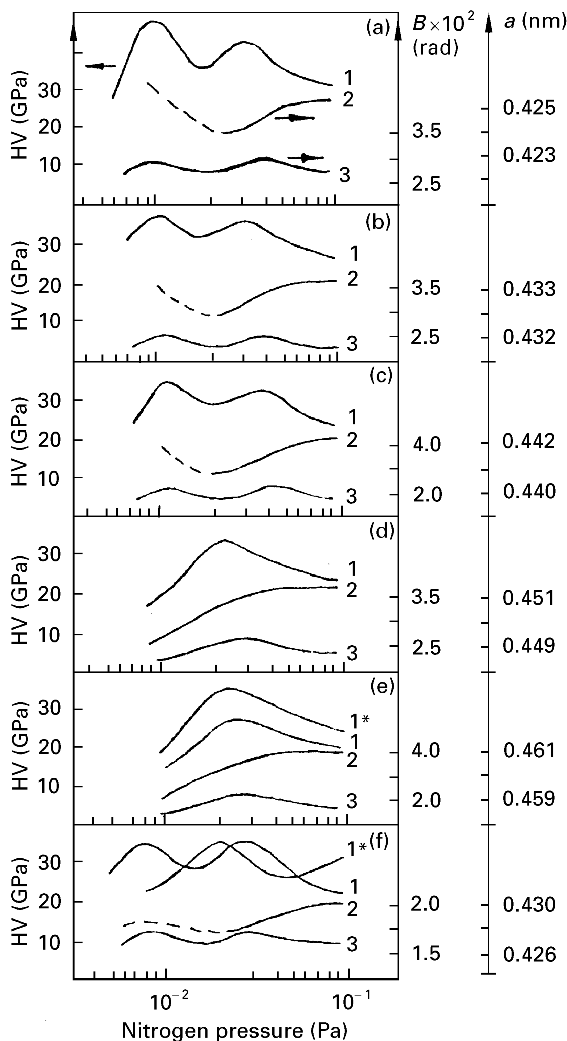

Figure 16 Effect of nitrogen pressure in the process deposition on (curves 1) hardness HV, lattice paramter *a* (curves 2), and full width at half-maximum B (curves 3) of films: (a) Ti–N; (b) Ti–25 wt % Zr–N; (c) Ti–50 wt % Zr–N; (d) Ti–75 wt % Zr–N; (e) Zr–N (curve 1*–Zr–2 wt % Nb–N); (d) Ti–21 wt % Mo–N (curve 1*–Ti–31 wt % Mo–N). Dotted lines (see (a), (b), (c) and (f)) show the value of the lattice period for the range of existence for tetragonal phases calculated by means of the formula which is used for cubic modifications [177].

tetragonal phase in the Zr–N system. The behaviour is also complicated in films based on the Ti–Mo–N system (Fig. 16f). For Ti–21 wt % Mo films the situation is similar to the case of Ti–Zr (50 wt % or less). For Ti–31 wt % Mo films the b.c.c. Ti–Mo–N phase has been shown to be in the region with low nitrogen content.

3. Some of the results of Table IX were obtained by nanoindentation tests (e.g. [122, 153, 155, 175]). These values may be low in comparison with conventional determinations because of possible known relaxation effects although in this case the substrate influence is essentially eliminated. Some other feature of the nanoindentation technique possibly caused additional scatter in the results such as the roughness of as-deposited surfaces (see Figs 7–9).
4. Although there are some questions over the Hall–Petch relation validity (see Figs 12 and 13 as well as results [178]), it seems that the question of the grain size effect remains to be clarified before detailed systematic knowledge can be obtained, especially as applied to representative grain size characterization. For example, nanoindentation testing of a CVD TiN film, consisting of ~ 10 nm grains and obtained by deposition on a (1 0 0) silicon substrate at 623 K from tetrakis titanium with ammonia, produced a hardness value only of 12.7 GPa [179]. This seems to be the minimum result recorded (see also [56]) and demands to be explained by a very small grain size as indicated above. Such an unclear situation is also the case [167, 168] for WC films.
5. As indicated above, alloying tends to increase the hardness such as in the case of (Ti,Al)N, (Ti,V)N, (Ti,Nb)N, (Ti,Zr)N, and (Ti,Zr)C films. The existence of oxygen tends as a rule to decrease the hardness. The effect of nitrogen and carbon atoms is considered to be additive. A very interesting situation was observed in (Ti,Zr)C and (Ti,Zr)N alloys [157, 161]. Annealing these films at 1000–1200 °C tends to increase the hardness, possibly the result of spinodal decomposition of the TiN–ZrN and TiC–ZrC systems with the formation of a nanocrystalline structure. Fig. 17 illustrates the dependence of the hardness of various films on the vacuum annealing temperature. The anomalous character of the (Ti,Zr)N film behaviour is evident.

These data also show that multilayer films are beneficial in comparison with alloyed and monolayer films. Compositional or multilayer (superlattice) films including those based on IPs, have long drawn attention (e.g. [84, 169, 180]). Their interesting properties such as hardness and wear resistance have been demonstrated in several systems: TiC/TiB_2, SiC/TiC, B_4C/TiB_2 etc. [169, 180, 181], TiN/ZrN, TiN/NbN, and TiN/CrN [100, 157, 184], TiN/VN, TiN/NbN, and TiN/(Nb,V)N [84, 158], TiN/Si_3N_4 [182], and TiN/CN_x [183]. Technology perspectives on CVD/PVD layer combinations have been discussed by Quinto [185].

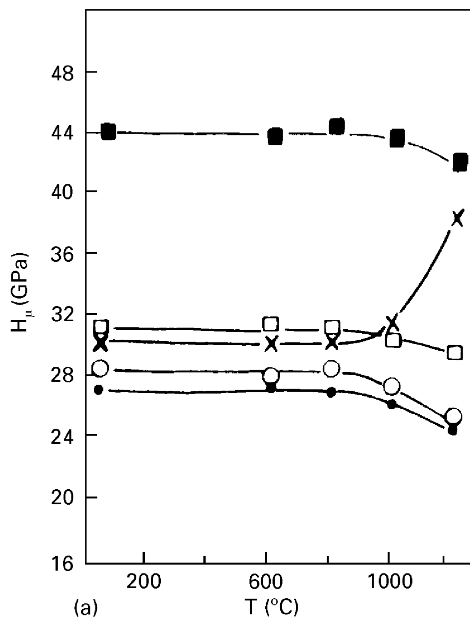

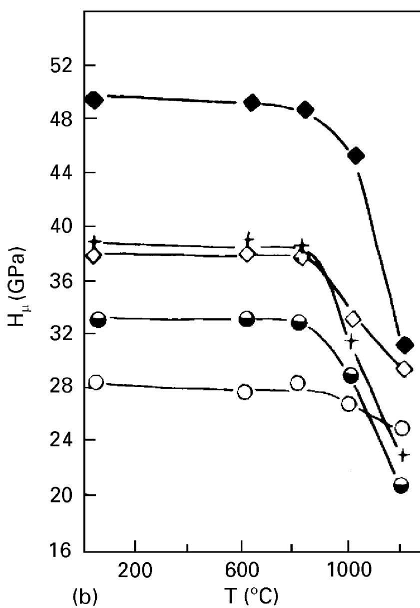

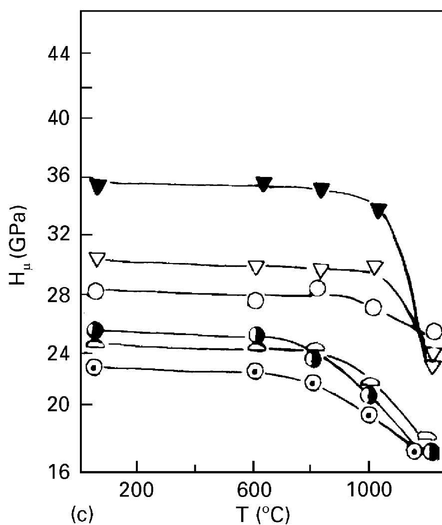

Figure 17 Hardness of films deposited by CAPD (thickness of 2 μm) as a function of annealing temperature: (a) (Ti, Zr) N; (b) (Ti, Nb) N; and (c) (Ti, Cr)N [157]. Key: (a) ■ TiN–ZrN 20 layers, □ TiN–ZrN 10 layers, × (TiZr)N, ○ TiN, • ZrN; (b) ◆ TiN–NbN 20 layers, ◇ TiN–NbN 10 layers, + (TiNb)N, ○ TiN, ◒ NbN; (c) ○ TiN, ⊙ CrN, ◑ Cr_2N, △ (TiCr)N, ▼ TiN–CrN 20 layers, ▽ TiN–CrN 10 layers.

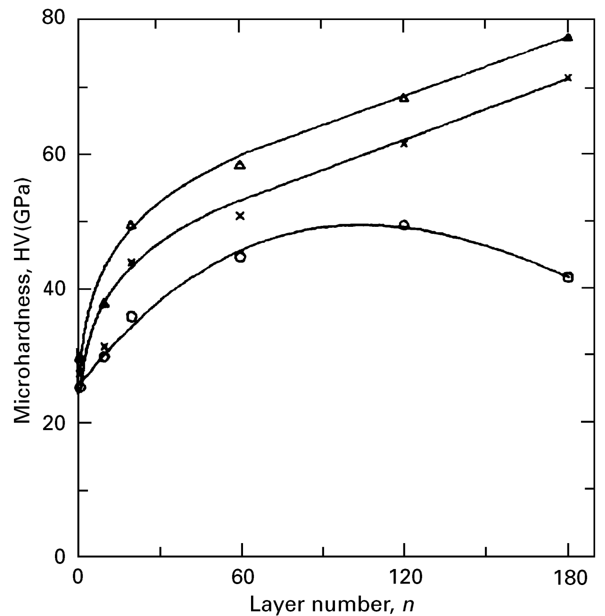

Figure 18 Influence of the number of layers on the nitride film's hardness [100]. Key: △ TiN–NbN, × TiN–ZrN, and ○ TiN–CrN.

Fig. 18 shows the influence of a number of layers on the hardness of TiN/ZrN, TiN/NbN, and TiN/CrN films which had a similar total thickness (nearly 2 μm) [100, 184]. There are at least four physical reasons for the observed hardness increase: (i) interphase boundaries stop crack propagation; (ii) the crystallite size has a low value in monolayers (equal to, near to or smaller than the layer thickness); (iii) the dislocation density increases as the result of the layer lattice mismatch; and (iv) possibly a more favourable situation exists with residual strains in multilayer films. The variable influence in the case of TiN/CrN films is connected with the (Ti,Cr) N solution formation for a number of layers greater than 100–120 which has been shown by XRD analysis. This fact also confirms the effects of interphase boundaries and layer lattice mismatch on increasing hardness. The high hardness nature of nitride superlattices has been discussed by Barnett (e.g. [84]).

It is also very interesting that the high hardness values of TiN/NbN and TiN/ZrN multilayer films disappeared after a period of time. The relaxation effect in superlattice nitride films has also been observed by Hultman *et al.* [85] as was mentioned early. Unfortunately we have not fixed exact time of decreasing hardness and a more complete data base will be required to develop the theory of this phenomenon.

High-temperature hardness of TiN, HfN, ZrN, (Ti,Al)N and TiC/TiB_2 films has been studied up to 1000 °C [165, 186]. While at 1000 °C all the hardness values of nitride films were separated by less than 1–2 GPa (∼8–10 GPa), for TiB_2, TiC and TiB_2/TiC films this difference at 900 °C was markedly greater (∼20 GPa for TiB_2–20%TiC and ∼9 GPa for TiB_2–50%TiC). Possibly in the case of TiB_2/TiN films this is connected with a display of superplasticity in nanocrystalline two-phase composites [17, 32, 33].

TABLE X Elastic properties of the IP films. Measuring methods: 1, flexural resonance frequency; 2, nanoindentation testing; 3, X-ray residual stress measurement; 4, Brillouin scattering

Phase	Preparation Method	Thickness (μm)	Texture	Measuring method	Modulus (GPa)		Poisson's ratio
					Elastic	Shear	
$TiN_{1.0}$ [188]	DCMRS	4–6	(2 2 0)	1	637		
$TiN_{0.5\text{–}1.0}$ [153]	DCMRS	5		2	300–450		
TiN_x [189]	DCMRS	5	(3 1 1), (2 0 0)	3			0.30
$TiN_{0.97}$ [190]	DCMRS	0.2–1.0	(1 1 1)	2	550 ± 50		
$TiN_{\sim 0.8}$ [191]	IBAD	0.3–0.9		2	~ 450		
$TiN_{\sim 0.8}$ [191]	IBAD	0.3–0.9		4		~ 130	
$TiN_{0.8}$ [175]	RFMRS	1–3		2	410		
TiN_x [192]	DCMRS	2		4		~ 192	
TiN_x [193]	CAPD	2		2	370 ± 81		
$ZrN_{\sim 1.0}$ [188]	DCMRS	4–6	(1 1 1)	1	460		
ZrN_x [189]	DCMRS	5	(2 0 0), (1 1 1)	3			0.19
$HfN_{\sim 1.0}$ [188]	DCMRS	4–6	(3 1 1)	1	380		
HfN_x [189]	DCMRS	5	(3 1 1), (1 1 1)	3			0.35
VN_x [192]	DCMRS	2		4		~ 149	
NbN_x [192]	DCMRS	2		4		~ 142	
(V,Nb) N_x [192]	DCMRS	2		4		~ 124	
(Ti,Al) N_x [193]	CAPD	2		2	298 ± 72		
(Ti,Nb) N_x [193]	CAPD	2		2	375 ± 43		
Ti $(C,N)_x$ [193]	CAPD	2		2	300 ± 30		
$TiC_{\sim 1.0}$ [188]	DCMRS	4–6	(1 1 1)	1	460		
$TiB_2N_{0.6}$ [175]	RFMNRS	1–3		2	640		
$TiB_{1.4}N_{0.5}$ [175]	RFMNRS	1–3		2	750		
$TiBN_{0.4}$ [175]	RFMNRS	1–3		2	500		
$TiB_{0.7}N_{0.5}$ [175]	RFMNRS	1–3		2	453		
$TiB_{0.6}N_{0.5}$ [175]	RFMNRS	1–3		2	276		

As is evident from the above account, the study of film hardness is important for many scientific and engineering purposes. To this we can add the different scratch testing methods by indentation for adhesion studies with fixed scratch test parameter (L_c, critical load of cohesive failure), microbrittleness and fracture toughness investigations (e.g. [24, 25, 187]). However, we have no possibility of analysing these questions because of limited review volume.

Table X shows values of elastic properties. When analysing Table X it is well to bear in mind that different measuring methods (see, for example, reviews [151, 152]) and preparation techniques as well as strong crystallographic texture in the films can effect the values of elastic properties. From these data the most representative values seem to be the results [188] for stoichiometric TiN, ZrN, and HfN. So for $TiN_{1.0}$ and $ZrN_{1.0}$, the Young's modulus values are in good agreement with an extensive study of fully dense specimens made by Portnoi *et al.* [194]. As in the case of hardness, a continuous indentation technique, consisting of the analysis of the indentation unloading curve, is now very popular for film investigations. However, not all results obtained (e.g. [193]) can be explained in detail as regards absolute values. We call attention also to the very high E values for some Ti–B–N films [175]. It is also interesting that decreasing the deposition temperature from 400 to 20 °C leads to a decrease in E of ~ 1.5 times ($TiBN_{0.5}$ composition). As has been indicated [193], heat treatment of deposited films is accompanied by increasing Young's modulus (maximum values were after ~ 500 °C) with a following decrease.

Attempts to reveal some significant anomalies in the elastic modulus of nitride superlattices have not been successful because the results [195] showed no evidence of anomalous elastic behaviour in the region with the highest hardness for $TiN/V_{0.3}Nb_{0.7}N$ superlattices.

4.4. Other properties

There are many investigations of tribological behaviour and corrosion performance of IP films (e.g. [24, 25, 28, 110, 111, 185, 196–199]). However, these aspects are not discussed in the present review. At the same time physico-chemical problems, such as phase equilibria, diffusion and diffusion-controlled processes, thermodynamics, deformation mechanisms and some others, have been studied on a very limited scale (e.g. [32, 33, 200]). To our knowledge, information on diffusion is limited to the diffusion barrier property studies (e.g. [201, 202]) and on thermodynamic parameters of $VH(D)_x$ film investigations [203].

A fractured cross-section specimen preparation technique through hardness indentation and scratch tests (see Fig. 7) [109] seems to be very promising for the examination of deformation and failure mechanisms in films. These investigations are in their early stages. There is some information on thermal stability and recrystallization of IP films including multilayer and nanocomposite ones (e.g. [89, 157, 161, 165, 184, 186, 193, 204–206]; see also Fig. 17).

It is common knowledge that formation of grains and recrystallization begin with the deposition

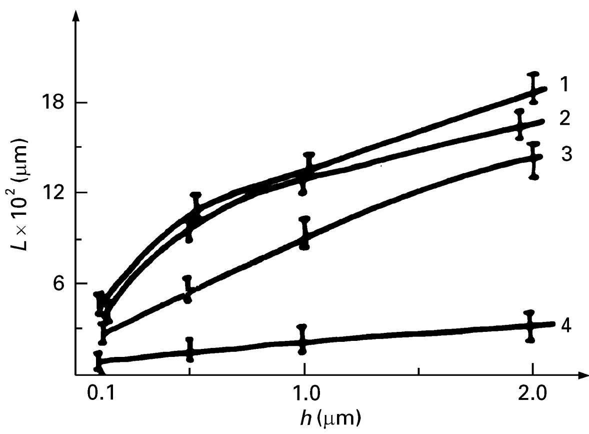

Figure 19 Grain size as a function of the film thickness: (1) TiN; (2) CrN; (3) NbN; (4) ZrN [206].

process. Fig. 19 shows the effect of film thickness on grain size for different nitrides prepared by CAPD. It is evident that there is a sharp influence in the case of TiN, CrN, and NbN films and a negligible influence on ZrN films. This difference remains to be studied, but possibly it may be connected with the greater activity of zirconium to nitrogen and the greater energy of the Zr ion. It is also interesting that the smallest L values were observed for multilayer ($n = 10$–20 layers) and alloyed films (Table XI) [206]. It is clear from Table XI, in the case of TiN/CrN multilayer and (Ti,Cr)N alloyed films, the L values are identical and do not vary from those for unalloyed TiN and CrN films. We have pointed out earlier (see Fig. 18) that in TiN/CrN multilayer films the formation of a (Ti, Cr)N solid solution had taken place and interphase boundaries had disappeared. The L values in TiN/NbN(ZrN, AlN) multilayer films are 2–4 or more times lower than those for individual nitride films.

It is notable that L values in alloyed films are correlated with the mixing energy E_{mix} in these nitride systems. From general considerations, this correlation may probably be connected with known low diffusion activity (and accordingly low recrystallization activity) in the solid solution with high level E_{mix} values.

Recrystallization features at a heat treatment up to 1000 °C for individual, alloyed and multilayer films have been studied in TiN, ZrN, NbN, AlN, and CrN films [157, 184, 204, 206]. For example, Figs 20 and 21 show the influence of thickness, number of layers and

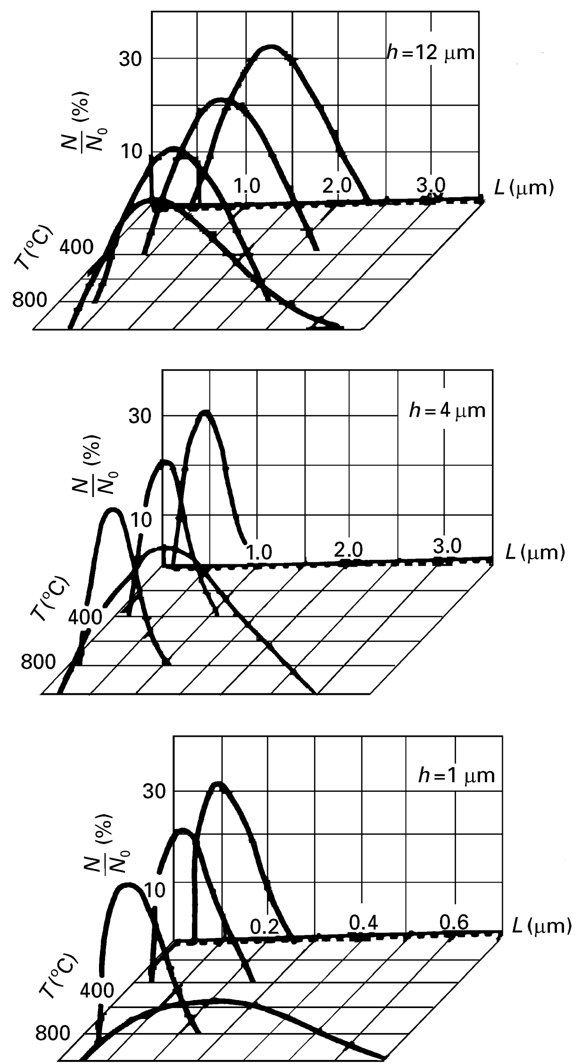

Figure 20 Statistical distributions of grain sizes for TiN films [157].

alloying for TiN and NbN films. The start of recrystallization is practically the same for TiN, NbN and ZrN films. However, for the former L values the dispersion appears lower and the coalescence mechanism is likely to be much more marked in the case of ZrN films. It is obvious that the recrystallization rate at 1000 °C ($t = 20$ min) is higher in the case of TiN thin films (1μm) relative to the thicker films (12 μm). The same situation of thickness influence is observed in NbN and other films. In multilayer films the recrystallization rate was distinctly smaller than that in monolayer films. This may be due to the restraining

TABLE XI The average L values of different nitride films (total thickness of 2 μm)

Nitride	L (μm)			E_{mix} in (Ti, M)N systems (kJ mol^{-1})
	Unalloyed films	Multilayer films (TiN/MN)	Alloyed films (Ti, M)N	
TiN	0.18 ± 0.08	–	–	–
CrN	0.16 ± 0.08	0.17 ± 0.05	0.18 ± 0.04	3.4
NbN	0.14 ± 0.03	0.04 ± 0.01	0.08 ± 0.02	6.1
ZrN	0.03 ± 0.02	~ 0.01	0.02 ± 0.01	32.6
AlN	0.15 ± 0.05	0.08 ± 0.03	~ 0.01	37.2

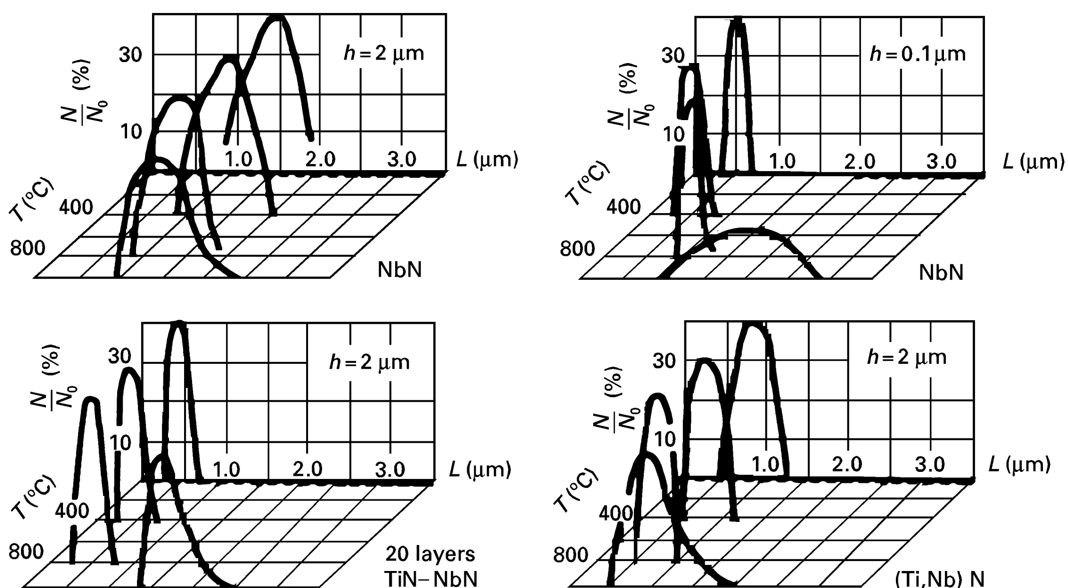

Figure 21 Statistical distributions of grain sizes of NbN, NbN/TiN and (Nb, Ti)N films [206].

role of the interphase boundaries in multilayer subjects. The alloying influence on recrystallization of (Ti, Nb)N films was not so great although in the case of (Ti, Zr)N and (Ti, Al)N (see Table XI) this effect is more significant. The details of the high-temperature behaviour of alloyed, multilayer and nanocomposite films need further investigation.

5. Conclusion

As is evident from the foregoing, the information on preparation, structure and properties of IP films is very comprehensive but not uniform. The largest body of information is related to nitrides especially to TiN, whereas very little data has been published on hydrides. Our review does not cover all details because of limited space but the present author has endeavoured to point out the main and unresolved aspects of this field. Previously a broad spectrum of application, such as tool materials, microelectronics, and decorative techniques has been considered. It seems to be clear that the development of next generation materials based on IP films is closely connected with the achievements of material science in nanocrystalline states. Many questions, such as the role of grain size, the nature of grain boundaries, the effects of impurities, the optimal phase equilibria and structure, need more theoretical and experimental studies to further the understanding of IP films, their processing behaviour, structure and final properties that will enable their large scale use.

Note added in proof. Since this paper was written further papers relating to the films of interstitial phases have been published [207–212]. This reflects a growing interest in this topic.

Acknowledgements

The author should like to express its appreciation to Drs I. A. Anisimova, V. P. Anisimov, I. A. Belokon', G. V. Kalinnikov, V. P. Makarov and Z. Kh. Fuksman for their help in this work. The author is grateful to the Russian Basic Research Foundation (grant 95-02-03518) and the INTAS Program (grant 94-1918) for support.

References

1. G. HAGG, *Z. Phys. Chem.* **B12** (1931) 33.
2. R. A. ANDRIEVSKI and YA. S. UMANSKI, "Interstitial phases" (Nauka, Moscow, 1977) (in Russian).
3. G. V. SAMSONOV and YA. S. UMANSKI, "Hard compounds of high-melting metals" (Metallurgija, Moscow, 1957) (in Russian).
4. H. J. GOLDSCHMIDT, "Interstitial alloys" (Plenum, New York, 1967).
5. E. K. STORMS, "The refractory carbides" (Academic, New York, 1967).
6. G. V. SAMSONOV, "Nitrides" (Naukova Dumka, Kiev, 1969) (in Russian).
7. L. E. TOTH, "Transition metal carbides and nitrides" (Academic, New York, 1971).
8. G. V. SAMSONOV, V. S. NESHPOR and G. S. UPADHYAYA, "Physical material science of carbides" (Naukova Dumka, Kiev, 1974) (in Russian).
9. YU. V. LEVINSKI, "Phase diagrams of metals with gases" (Metallurgija, Moscow, 1975) (in Russian).
10. A. A. SMIRNOV, "Theory of interstitial alloys" (Nauka, Moscow, 1979) (in Russian).
11. YU. B. KUZ'MA, "Crystal chemistry of borides" (Vischa Shkola, L'vov, 1983) (in Russian).
12. H. HOLLECK, "Binare und ternare carbid- und nitridsysteme der Ubergangsmetalle" (Gebruder Borntrager, Berlin, 1984).
13. G. P. SHVEIKIN, S. I. ALIAMOVSKI, YU. G. ZAINULIN and A. I. GUSEV, "Compounds of variable composition and their solid solutions" (UNTS AN SSSR, Sverdlovsk, 1984) (in Russian).
14. P. V. ZUBAREV, "High-temperature strength of interstitial phases" (Metallurgija, Moscow, 1985) (in Russian).
15. R. A. ANDRIEVSKI, "Materials science of hydrides" (Metallurgija, Moscow, 1986) (in Russian).
16. A. I. GUSEV and A. A. REMPEL, "Structural and phase transitions in nonstoichiometric compounds" (Nauka, Moscow, 1988) (in Russian).
17. R. A. ANDRIEVSKI and I. I. SPIVAK, "Strength of high-melting compounds and related materials" (Metallurgija, Cheliabinsk, 1989) (in Russian).

18. E. A. ZHURAKOVSKI and V. F. NEMCHENKO, "Kinetic properties and electronic structure of interstitial phases" (Naukova Dumka, Kiev, 1989) (in Russian).
19. T. I. SEREBRIAKOVA, V. A. NERONOV and P. D. PESHEV, "High-melting point borides" (Metallurgija, Moscow, 1991) (in Russian).
20. A. I. GUSEV, "Physical chemistry of nonstoichiometric high-melting compounds" (Nauka, Moscow, 1991) (in Russian).
21. V. A. GUBANOV, A. L. IVANOVSKIY and V. P. ZHUKOV, "Electronic properties of refractory carbides and nitrides of the transition metals" (Cambridge University Press, Cambridge, 1994).
22. J.-E. SUNDGREN, *Thin Solid Films* **128** (1985) 21.
23. K. REICHELT and X. JIANG, *ibid.* **191** (1990) 91.
24. D. S. RICKERBY and A. MATTHEWS, *Rev. Powder Metall. Phys. Ceram.* **4** (1991) 155.
25. S. CHATTERJEE, T. S. SUDARSHAN and S. CHANDRASHEKHAR, *J. Mater. Sci.* **28** (1993) 1989.
26. J. MUSIL, J. VYSKOČIL and S. KADLEC, "Physics of thin films. mechanic and dielectric properties", Vol. 17, edited by M. H. Francombe and J. L. Vossen (Academic Press, New York, 1993) pp. 79–144.
27. H. REBENNE and D. G. BHAT, *Surf. Coating Technol.* **63** (1994) 1.
28. M. G. HOCKING, V. S. VASANTASREE and P. S. SIDKY, "Metallic and ceramic coatings: production, high-temperature properties and applications" (Longman, Harlow, 1989).
29. A. V. BYELI, G. D. KARPENKO and N. K. MYSHKIN, "Structure and formation methods of wear-resisistant surface layers" (Mashinostroenie, Moscow, 1991) (in Russian).
30. V. V. KUDINOV and G. V. BOBROV, "Vapour deposition of coatings. theory, engineering and equipment" (Metallurgija, Moscow, 1992) (in Russian).
31. M. KONUMA, "Film deposition by plasma techniques" (Springer Verlag, Berlin, 1992).
32. R. A. ANDRIEVSKI, *J. Mater. Sci.* **29** (1994) 614.
33. R. A. ANDRIEVSKI, *Russ. Chem. Rev.* **63** (1994) 411.
34. R. F. BUNSHAH, *IEEE Trans. Plasma Sci.* **18** (1990) 846.
35. R. F. BUNSHAH, R. NIMMAGADDA, W. DUNFORD, B. A. MOVCHAN, A. V. DEMCHISHIN and N. A. CHURSANOV, *Thin Solid Films* **54** (1978) 85.
36. R. F. BUNSHAH and C. V. DESHPANDEY, *J. Vac. Sci. Technol.* **A 3** (1985) 553.
37. A. I. GOLOVASHKIN, B. G. ZHURKIN, A. L. KARUZSKII, S. I. KRASNOSVOBODTSEV, V. P. MARTOVITSKIY, E. V. PECHEN, V. V. RODIN, YU. I. STEPANOV and A. V. SHIRKOV, *Solid State Phys.* **28** (1986) 3342 (in Russian).
38. S. K. SINGH, K. RAMAKRISHNA, A. K. SINGH and O. N. SRIVASTAVA, *Int. J. Hydrogen Energy* **14** (1989) 573.
39. J. LI and Y.-T. CHENG, *J. All. Comp.* **223** (1995) 6.
40. D. M. MATTOX and J. E. McDONALD, *J. Appl. Phys.* **34** (1963) 2493.
41. H. RANDHAWA, *Thin Solid Films* **196** (1991) 329.
42. A. M. DORODNOV, *J. Techn. Phys.* **48** (1978) 1858 (in Russian).
43. I. I. AKSENOV, V. G. BREN', V. G. PADALKA and V. M. KHOROSHIKH, *ibid.* **48** (1978) 1165 (in Russian).
44. P. J. MARTIN, R. P. NETTERFIELD and T. I. KINDER, *Thin Solid Films* **193** (1990) 77.
45. O. KNOTEK, F. LOFFLER and G. KRAMER, *Surf. Coating Technol.* **59** (1993) 14.
46. A. MATTHEWS, K. S. FANCEY, A. S. JAMES and A. LEYLAND, *ibid.* **61** (1993) 121.
47. J. S. COLLIGON, *Mater. Sci. Engng* **A139** (1991) 199.
48. X. Y. LI, F. J. WANG, T. C. MA and Y. K. WANG, *ibid.* **A139** (1991) 225.
49. J. P. RIVIERE, Ph. GUESDON, J. DELAFOND, M. F. DENANOT, G. FARGES and D. DEGOUT, *Thin Solid Films* **204** (1991) 151.
50. C. D. TSIOGAS and J. N. AVARITSIOTIS, *Vacuum* **43** (1992) 203.
51. A. V. BYELI and S. A. FEDOTOV, *Surf. Engng* **10** (1994) 136.
52. K. BARTSCH, A. LEONHARDT, E. WOLF and M. SCHONHERR, *J. Mater. Sci.* **26** (1991) 4318.
53. K.-T. RIE and A. GEBAUER, *Mater. Sci. Engng* **A139** (1991) 61.
54. H. FRELLER and H. P. LORENZ, *ibid.* **A140** (1991) 534.
55. C. I. M. A. SPEE, J. P. A. M. DRIESSEN and A. D. KUYPERS, *J. Phys. IV*, *Colloq. C5* **5** (1995) 719.
56. L. X. CAO, Z. C. FENG, Y. LIANG, W. L. HOU, B. C. ZHANG, Y. Q. WANG and L. LI, *Thin Solid Films* **257** (1995) 7.
57. H. TSUDA and Y. NUMASAWA, *Jpn J. Appl. Phys.* **34** (1995) L691.
58. A. WEBER, R. NIKULSKI, C.-P. KLAGES, M. E. GROSS, W. L. BROWN, E. DONS and R. M. CHARATAN, *J. Electrochem. Soc.* **141** (1994) 849.
59. M. BOUMERZOUG, P. MASCHER and J. G. SIMMONS, *Appl. Phys. Lett.* **66** (1995) 2664.
60. A. WEBER, R. POELCKELMANN and C.-P. KLAGES, *ibid.* **67** (1995) 2934.
61. R. FIX, R. G. GORDON and D. M. HOFFMAN, *Chem. Mater.* **3** (1991) 1138.
62. R. FIX, R. G. GORDON and D. M. HOFFMAN, *ibid.* **5** (1993) 614.
63. M. RITALA, M. LESKELA, E. RAUHALA and P. HAUSSALO, *J. Electrochem. Soc.* **142** (1995) 2731.
64. J. A. JENSEN, J. E. GOZUM, D. M. POLLINA and G. S. GIROLAMI, *J. Amer. Chem. Soc.* **110** (1988) 1643.
65. A. L. WAIDA, L. F. SCHNEEMEYER, R. L. OPILA, *Appl. Phys. Lett.* **53** (1988) 361.
66. R. A. ANDRIEVSKI, S. E. KRAVCHENKO and S. P. SHILKIN, Proceedings of the 11th International Symposium on Boron, Borides and Related Compounds, Tsukuba, 1993, edited by R. Uno and I. Higashi, JJAP Series 10 (JJAP, Tokyo, 1994)p. 198.
67. H. ZHENG, K. OKA and D. MACKENZIE, "Better ceramics through chemistry. V", Vol. 27, edited by M. J. Hampden-Smith, W. G. Klemperer and C. J. Brinkes (MRS, Pittsburgh, 1992) p. 893.
68. K. YABE, O. NISHIMURA, T. FUJIHANA and M. IWAKI, *Surf. Coating Technol.* **66** (1994) 250.
69. Y. KASUKABE, J. OOTUBO, SH. NAGATA, M. KISHIMOTO, Y. FUINO, S. YAMAGUCHI and Y. YAMADA, *Jpn J. Appl. Phys.* **34** (1995) 3234.
70. T. SHIBUTAMI, Y. KANZAKI and O. MATSUMOTO, *J. Less-Common Met.* **113** (1985) 177.
71. K. W. VOGT, L. A. NAUGHER and P. A. KOHL, *Thin Solid Films* **256** (1995) 106.
72. I. P. JAIN, Y. K. VIJAY, K. S. UPADHYAY and M. SINGH, *Int. J. Hydrogen Energy* **15** (1990) 345.
73. H. SAKAGUCHI, T. TSUJIMOTO and G. ADACHI, *Chem. Mater.* **5** (1993) 6.
74. J.-P. NOEL, D. C. HOUGHTON, G. ESTE, F. R. SHEPHERD and H. PLATTNER, *J. Vac. Sci. Technol.* **A2** (1984) 284.
75. O. KNOTEK, M. BOHMER, T. LEYENDECKER and F. JUNGBLUT, *Mater. Sci. Engng* **A105/106** (1988) 481.
76. P. PANJAN, B. NAVINSEK, A. ZABKAR, J. FISER and A. ZALAR, *Vacuum* **40** (1990) 81.
77. R. LOHMANN, E. OSTERSCHULZE, K. THOMA, H. GARTNER, W. HERR, B. MATTHES, E. BROSZEIT and K.-H. KLOOS, *Mater. Sci. Engng* **A139** (1991) 259.
78. M. YOSHITAKE, T. YOTSUYA and S. OGAWA, *Jpn J. Appl. Phys.* **31** (1992) 4002.
79. R. A. ANDRIEVSKI, G. V. KALINNIKOV, A. F. POTAFEEV, M. A. PONOMAREV and S. YU. SHARIVKER, *Inorg. Mater.* **31** (1995) 1536 (in Russian).
80. N. EGUCHI, V. GRAJEWSKI, H. H. UCHIDA and E. FROMM, *Mater. Sci. Engng* **A139** (1991) 339.
81. B. O. JOHANSSON, H. T. G. HENTZELL, J. M. E. HARPER and J. J. CUOMO, *J. Mater. Res.* **1** (1986) 442.
82. T. P. MOLLART, B. BAKER, J. HAUPT, A. STEINER, P. HAMMER and W. GISSLER, *Surf. Coating Technol.* **74–75** (1995) 491.
83. J. A. SUE, *ibid.* **61** (1993) 115.

84. S. A. BARNETT, "Physics of thin films. mechanic and dielectric properties", Vol. 17, edited by M. H. Francombe and J. L. Vossen (Academic Press, New York, 1993) p. 1.
85. L. HULTMAN, M. SHINN, P. B. MIRKARIMI and S. A. BARNETT, *J. Cryst. Growth* **135** (1994) 309.
86. C. JIANG, T. GOTO and T. HIRAI, *J. Mater. Sci.* **29** (1994) 669.
87. V. VALVODA, *J. All. Comp.* **219** (1995) 83.
88. D. WANG, X. WANG, G. YANG, X. LIU, Y. JIA, G. ZHOU and G. LI, *J. Appl. Phys.* **77** (1995) 2945.
89. J. CHEN and J. A. BARNARD, *Mater. Sci. Engng* **A191** (1995) 233.
90. W. LENGAUER, *J. All. Comp.* **186** (1992) 293.
91. A. J. PERRY, *J. Vac. Sci. Technol.* **A6** (1988) 2140.
92. R. M. MANORY and G. KIMMEL, *Surf. Coating Technol.* **63** (1994) 85.
93. J. BRUNNER and A. J. PERRY, *Thin Solid Films* **153** (1987) 103.
94. J. P. SCHAFFER, A. J. PERRY and J. BRUNNER, *ibid.* **A10** (1992) 193.
95. A. UEDONO, S. NANAO, SH. TANIGAWA, R. SUZUKI, T. OHDAIRA, T. MIKADO and Sh. ISHIBASHI, *Jpn J. Appl. Phys.* **34** (1995) 5711.
96. E. V. SHALAEVA, M. V. KUZNETSOV, R. S. BARYSHEV and B. V. MITROFANOV, *J. Phys. IV suppl.* **1** (1991) C2-209.
97. A. LAOR, L. ZEVIN, J. PELLEG and N. CROITORU, *Thin Solid Films* **232** (1993) 143.
98. N. HAYASHI, I. H. MURZIN, I. SAKAMOTO and M. OHKUBO, *ibid.* **259** (1995) 146.
99. L. HULTMAN, U. HELMERSSON, S. A. BARNETT, J.-E. SUNDGREN and J. E. GREENE, *J. Appl. Phys.* **61** (1987) 552.
100. R. A. ANDRIEVSKI, I. A. ANISIMOVA and V. P. ANISIMOV, *Phys. Chem. Mater. Proc.* (2) (1992) 99 (in Russian).
101. U. C. OH, J. H. JE and J. Y. LEE, *J. Mater. Res.* **10** (1995) 634.
102. H. H. YANG, J. H. JE and K.-B. LEE, *J. Mater. Sci. Lett.* **14** (1995) 1635.
103. Y. GENQING, W. DAZHI, L. XIAGHUAI, W. XI and Z. SHICHANG, *Surf. Coating Technol.* **65** (1994) 214.
104. H. YUMOTO, K. KANEKO, M. ISHIHARA, K. AKASI and T. KANEKO, *Adv. Mater. Opt. Electron* **5** (1995) 191.
105. V. VALVODA and J. MUSIL, *Thin Solid Films* **149** (1987) 49.
106. D. MAHEO and J.-M. POITEVIN, *ibid.* **237** (1994) 78.
107. H. G. JIANG, H. Y. TONG, K. LU, B. Z. DING, Q. H. SONG and Z. Q. HU, "Advanced materials '93, I/A: Ceramics, powders, corrosion and advanced processing", Trans. Mat. Res. Soc. Jpn., Vol. 14A, edited by N. Mizutani *et al.* (Elsevier Science, Amsterdam, 1994) p. 785.
108. I. V. ALEKSANDROV and R. Z. VALIEV, *Phys. Met. Met. Sci.* **76** (1994) 77 (in Russian).
109. K. J. MA and A. BLOYCE, *Surf. Eng.* **11** (1995) 71.
110. I. EFEOGLU, R. D. ARNELL, S. F. TINSTON and D. G. TEER, *Surf. Coating Technol.* **57** (1993) 61.
111. E. BROSZEIT, B. MATTHES, W. HERR and K. H. KLOOS, *ibid.* **58** (1993) 29.
112. R. A. ANDRIEVSKI, "Fracture mechanics of ceramics", edited by R. C. Bradt, D. P. H. Hasselman, D. Munz, M. Sakai and V. Y. A. Shevchenko, Vol. 11 (Plenum Press, New York, 1996) p. 357.
113. K. L. WESTRA and D. J. THOMPSON, *Thin Solid Films* **257** (1995) 15.
114. R. HILLEL, M. MALINE, F. GOURBILLEAU, G. NOUET, R. CARLES and A. MLAYAH, *Mater. Sci. Engng* **A168** (1993) 183.
115. A. A. BABAD-ZAKHRIAPIN, "Defects in coatings" (Energoatomizdat, Moscow, 1987) (in Russian).
116. B. A. MOVCHAN and A. V. DEMCHISHIN, *Phys. Met. Met. Sci.* **28** (1969) 653 (in Russian).
117. J. A. TORNTON, *Ann. Rev. Mater. Sci.* **7** (1977) 239.
118. A. LEBUGLE, R. NYHOLM and N. MARTENSSON, *J. Less Common Met.* **82** (1981) 269.
119. M. V. KUZNETSOV, YU. F. ZHURAVLEV, D. L. NOVIKOV and V. A. GUBANOV, *Surf. Phys. Chem. Mech.* (1) (1990) 131 (in Russian).
120. R. P. NETTERFIELD, P. J. MARTIN and D. R. McKENZIE, *J. Mater. Sci. Lett.* **9** (1990) 972.
121. B. O. JOHANSSON, J.-E. SUNDGREN, J. E. GREENE, A. ROCKETT and S. A. BARNETT, *J. Vac. Sci. Technol.* **A3** (1985) 303.
122. A. BENDAVID, P. J. MARTIN, R. P. NETTERFIELD and T. J. KINDER, *Surf. Coating Technol.* **70** (1994) 97.
123. S. HORITA, T. TUJIKAWA, H. AKAHORI, M. KOBAYASHI and T. HATA, *J. Vac. Sci. Technol.* **A11** (1993) 2452.
124. R. NOWAK and S. MARUNO, *Mater. Sci. Engng* **A202** (1995) 226.
125. L. RIVAUD, S. BARNETT, J. GREENE and E. MARCINIEC, *J. Vac. Sci. Technol.* **A9** (1991) 2180.
126. K. K. SHIH and D. D. DOVE, *ibid.* **A8** (1990) 1399.
127. F. C. T. SO, E. KOLAWA, X.-A. ZHAO and M.-A. NICOLET, *Thin Solid Films* **153** (1987) 507.
128. J.-F. LEI, H. OKIMURA and J. O. BRITTAIN, *Mater. Sci. Engng* **A123** (1990) 129.
129. S. I. KRASNOSVOBODZEV, N. P. SHABANOVA, E. V. EKIMOV, V. S. NOZDRIN and E. V. PECHEN, *J. Exp. Theor. Phys.* **108** (1995) 970 (in Russian).
130. J. R. SHAPPIRIO and J. J. FINNEGAN, *Thin Solid Films* **107** (1983) 81.
131. J. G. RYAN, S. ROBERTS, G. J. SLUSSER and D. ADAMS, *ibid.* **153** (1987) 329.
132. W. Y. LEE, G. OLIVE, F. SEQUEDA, V. DELINE, T. HUANG, G. GORMAN and D. W. CHUNG, *ibid.* **166** (1988) 131.
133. J. G. RYAN and S. ROBERTS, *ibid.* **135** (1986) 9.
134. R. SPULAK, *J. Less-Common Met.* **160** (1990) 15.
135. K. H. SCHWARZ, A. R. WILLIAMS, J. J. CUOMO, J. M. E. HARPER and H. T. G. HENTZEL, *Phys. Rev.* **B8** (1985) 5489.
136. G. ADACHI, K. NIKI, H. NAGAI and J. SHIOKAWA, *J. Less-Common Met.* **88** (1982) 213.
137. H. SAKAGUCHI, Y. YAGI, N. TANIGUCHI, G. ADACHI and J. SHIOKAWA, *ibid.* **135** (1987) 137.
138. M. SINGH, *Int. J. Hydrogen Energy* **21** (1996) 223.
139. W. TSAI, M. DELFINO, J. A. FAIR and D. HODUL, *J. Appl. Phys.* **73** (1993) 4462.
140. M. J. DEEN, *Thin Solid Films* **152** (1987) 535.
141. N. HIRASHITA, J. E. GREENE, U. HELMERSSON, J. BICH and J.-E. SUNDGREN, *J. Appl. Phys.* **70** (1991) 4963.
142. Y. IGASAKI and H. MITSUHASHI, *Thin Solid Films* **70** (1980) 17.
143. L. ROUX, J. HANUS, J. C. FRANCOIS and M. SIGRIST, *Sol. Energy Mater.* **7** (1982) 299.
144. M. BONELLI, L. A. GUZMAN, M. MIOTELLO, L. CALLIARI, M. ELENA and P. M. OSSI, *Vacuum* **43** (1992) 459.
145. P. POLATO, H. FRANZ, F. RUSTICHELLI, M. MONTECCHI and A. PIEGARI, *Thin Solid Films* **248** (1994) 184.
146. L. LOGOTHETIDIS, I. ALEXANDROU and A. PAPADOPOULUS, *J. Appl. Phys.* **77** (1995) 1043.
147. B. JONSSON and S. HOGMARK, *Thin Solid Films* **114** (1984) 257.
148. A. A. VOEVODIN, S. E. SPASSKI and A. L. EROKHIN, *Industr. Labor.* **57** (1991) 45 (in Russian).
149. S. JA. BETSOFEN, *Metals* (2) (1993) 181 (in Russian).
150. T. F. PAGE and S. V. HAINSWORTH, *Surf. Coating Technol.* **61** (1993) 201.
151. E. D. NICHOLSON and J. E. FIELD, *J. Hard. Mater.* **5** (1994) 89.
152. E. SODERLUND and D. J. ROWCLIFFE, *ibid.* **5** (1994) 149.
153. W. C. OLIVER, C. J. McHARGUE and S. J. ZINKLE, *Thin Solid Films* **153** (1987) 185.
154. D. C. KOTHARI, P. SCARDI, S. GIALANIELLA and I. GUZMAN, *Phil. Mag.* **B61** (1990) 627.

155. E. SODERLUND and D. J. ROWCLIFFE, "Mechanical properties and deformation behavior of materials having ultra-fine microstructure", edited by M. Nastasi, D. M. Parkin and H. Gleiter (Kluwer Acad. Publ., Dordrecht, 1993) p. 463.
156. O. A. JOHANSEN, J. H. DONTJE and R. L. D. ZENNER, *Thin Solid Films* **153** (1987) 75.
157. R. A. ANDRIEVSKI, I. A. ANISIMOVA and V. P. ANISIMOV, *ibid.* **205** (1991) 171.
158. U. HELMERSSON, S. TODOROVA, S. A. BARNETT, J. -E. SUNDGREN, L. S. MARKERT and J. E. GREENE, *J. Appl. Phys.* **62** (1987) 481.
159. O. KNOTEK, W. BURGMER and C. STOESSEL, *Surf. Coating Technol.* **54/55** (1992) 249.
160. G. HAKANSSON, J. -E. SUNDGREN, D. McINTYURE, J. E. GREENE and W. -D. MUNZ, *Thin Solid Films* **153** (1987) 55.
161. O. KNOTEK and A. BARIMANI, *ibid.* **174** (1989) 51.
162. H. RANDHAWA, *ibid.* **153** (1987) 209.
163. Ch. TASCHNER, A. LEONHARDT, M. SCHNOHERR, E. WOLF and J. HENKE, *Mater. Sci. Engng* **A139** (1991) 67.
164. X.-M. HE, W.-ZH. LI and H.-D. LI, *J. Mater. Res.* **9** (1994) 2355.
165. H. HOLLECK and M. LAHRES, *Mater. Sci. Engng* **A140** (1991) 609.
166. A. K. DUA and V. C. GEORGE, *Thin Solid Films* **247** (1994) 34.
167. P. K. SRISTAVA, V. D. VANKAR and K. L. CHOPRA, *ibid.* **161** (1988) 107.
168. A. CAVALEIRO and M. T. VIEIRA, *Surf. Engng* **10** (1994) 147.
169. H. HOLLECK and H. SCHULZ, *Surf. Coating Technol.* **36** (1988) 707.
170. C. MITTERER, M. RAUTER and P. RODHAMMER, *ibid.* **41** (1990) 351.
171. W. HERR, B. MATTHES, E. BROSZEIT and K. H. KLOSS, *Mater. Sci. Engng* **A140** (1991) 616.
172. O. KNOTEK and F. LOFFLER, *J. Hard Mater.* **3** (1992) 29.
173. J. P. RIVIERE, PH. GUESDON, J. DELAFOND and M. F. DENANOT, *J. Less-Common Met.* **145** (1988) 477.
174. C. MITTERER, A. UBLEIS and R. EBNER, *Mater. Sci. Engng* **A140** (1991) 670.
175. P. HAMMER, A. STEINER, R. VILLA, M. BAKER, P. N. GIBSON, J. HAUPT and W. GISSLER, *Surf. Coating Technol.* **68/69** (1994) 194.
176. R. A. ANDRIEVSKI, I. A. BELOKON, V. V. KAPSHENINOV, V. P. MAKAROV, Z. KH. FUKSMAN and G. B. SHWETS, *Izv. Acad. Sci. Kirghiz. SSR, phys.-techn. mathem. ser.* No. 2 (1989) 32 (in Russian).
177. R. A. ANDRIEVSKI, I. A. BELOKON' and Z. KH. FUKSMAN, "High performance ceramic films and coatings", edited by P. Vincenzini (Elsevier, Amsterdam, 1991) p. 469.
178. K. MIURA, I. ISHIGAMI, M. KUNO and H. KANEDA, *J. Jpn Inst. Met.* **59** (1995) 303.
179. Y. W. BAE, W. Y. LEE, T. M. BESMANN and P. J. BLAU, *Appl. Phys. Lett.* **66** (1995) 1895.
180. B. A. MOVCHAN, A. V. DEMCHISHIN, G. F. BADILENKO, R. F. BUNSHAH, C. SANS, C. DESHPANDEY and H. J. DOERR, *Thin Solid Films* **97** (1982) 215.
181. G. HILZ and H. HOLLECK, *Int. J. Refr. Met. Hard Mater.* **14** (1996) 97.
182. S. VEPŘEK, S. REIPRICH and L. SHIZHI, *Appl. Phys. Lett.* **66** (1995) 2640.
183. D. LI, X. CHU, SH.-C. CHENG, X.-W. LIN, V. P. DRAVID, Y.-W. CHUNG, M.-SH. WONG and W. D. SPROUL, *ibid.* **67** (1995) 203.
184. R. A. ANDRIEVSKI, *Int. J. Refr. Met. Hard Mater.* **14** (1996) 105.
185. D. T. QUINTO, *ibid.* **14** (1996) 7.
186. D. T. QUINTO, G. J. WOLFE and P. C. JINDAL, *Thin Solid Films* **153** (1987) 19.
187. M. G. KARPMAN, R. KH. SAIDAKHMEDOV and G. P. FETISOV, *Industr. Labor.* **60** (1994) 40 (in Russian).
188. E. TOROK, A. J. PERRY, L. CHOLLET and W. D. SPROUL, *Thin Solid Films* **153** (1987) 37.
189. A. J. PERRY, *ibid.* **193/194** (1990) 463.
190. D. S. STONE, K. B. YODER and W. D. SPROUL, *J. Vac. Sci. Technol.* **A9** (1991) 2543.
191. X. JIANG, M. WANG, K. SCHMIDT, E. DUNLOP, J. HAUPT and W. GISSLER, *J. Appl. Phys.* **69** (1991) 3053.
192. P. B. MIKARIMI, M. SHINN, S. A. BARNETT, S. KUMAR and M. GRIMSDITCH, *ibid.* **71** (1992) 4955.
193. E. VANCOILLE, J. P. CELIS and J. R. ROOS, *Thin Solid Films* **224** (1993) 168.
194. K. I. PORTNOI, A. A. MUKASEEV, V. N. GRIBKOV and Yu. V. LEVINSKIY, *Powder Metall.* **N5** (1968) 87 (in Russian).
195. P. B. MIRKARIMI, S. A. BARNETT, K. M. HUBBARD, T. R. JERVIS and L. HULTMAN, *J. Mater. Res.* **9** (1994) 1456.
196. B. MATTHES, E. BROSZEIT and K. H. KLOOS, *Surf. Coating Technol.* **57** (1993) 97.
197. I. MILOSEV and B. NAVINSEK, *ibid.* **63** (1994) 173.
198. I. YU. KONYASHIN, *Thin Solid Films* **249** (1994) 174.
199. K. HOLMBERG and A. MATTHEWS, "Coatings tribology. Properties, techniques and application in surface engineering" (Elsevier, Amsterdam, 1994).
200. H. HOLLECK, *Surf. Coating Technol.* **36** (1988) 151.
201. M. OSTLING, S. NYGREN, C. S. PETERSSON, H. NORSTROM, R. BUCHTA, H.-O. BLOM and S. BERG, *Thin Solid Films* **145** (1986) 81.
202. D.-Y. SHIH, C.-A. CHANG, J. PARASZCZAK, S. NUNES and J. CATALDO, *J. Appl. Phys.* **70** (1991) 3052.
203. K. PAPATHANASSOPOULOS and W. WENZL, *J. Phys. F: Met. Phys.* **12** (1982) 1369.
204. R. A. ANDRIEVSKI, I. A. ANISIMOVA and V. P. ANISIMOV, *Inorg. Mater.* **28** (1992) 365 (in Russian).
205. F. GORBILLEAU, R. HILLEL and G. NOET, *Nanostruct. Mater.* **4** (1994) 215.
206. R. A. ANDRIEVSKI, I. A. ANISIMOVA, V. P. ANISIMOV, V. P. MAKAROV and V. P. POPOVA, *Thin Solid Films* **261** (1995) 83.
207. J. E. SUNDGREN and L. HULTMAN, "Materials and processes for surface and interface engineering", edited by Y. Pauleau (Klewer Academic, Dodrecht, 1995) p. 453.
208. J. HUIBERTS, R. GRIESSEN, J. H. RECTOR, W. J. WIJNGAARDEN, J. P. DECCER, D. G. GRROT, and N. J. KOEMAN, *Nature* (London) **380** (1996) 231.
209. C. MITTERER, H.-M. OTT, J. KOMENDA-STALLMAIER, P. SCHMOLZ, W. S. M. WERNER and H. STORI, *J. All. Comp.* **239** (1996) 183.
210. I. WADSWORTH, D. B. LEWIS and G. WILLIAMS, *J. Mater. Sci.* **31** (1996) 5907.
211. M. SHIWA, E. WEPPELMANN, D. MUNZ, M. V. SWAIN and T. KISI, *ibid.* **31** (1996) 5985
212. R. A. ANDRIEVSKI, *Russ. Chem. Rev.* **66** (1996) 57.

Received 30 April 1996
and accepted 10 February 1997